

# Flavorful Lepton Number Violation at the EIC

---

**Sebastián Urrutia Quiroga,<sup>a,b</sup> Vincenzo Cirigliano,<sup>a</sup> Wouter Dekens,<sup>a</sup> Kaori Fuyuto,<sup>c</sup>  
Emanuele Mereghetti<sup>d</sup>**

<sup>a</sup>*Institute for Nuclear Theory, University of Washington, Seattle, WA 91195-1550, USA*

<sup>b</sup>*Northwestern University, Department of Physics & Astronomy, 2145 Sheridan Road, Evanston, IL 60208, USA*

<sup>c</sup>*KEK Theory Center, IPNS, KEK, Tsukuba 305-0801, Japan*

<sup>d</sup>*Theoretical Division, Los Alamos National Laboratory, Los Alamos, NM 87545, USA*

*E-mail:* [suq90@uw.edu](mailto:suq90@uw.edu), [cirigv@uw.edu](mailto:cirigv@uw.edu), [wdekens@uw.edu](mailto:wdekens@uw.edu), [kfuyuto@post.kek.jp](mailto:kfuyuto@post.kek.jp),  
[emereghetti@lanl.gov](mailto:emereghetti@lanl.gov)

**ABSTRACT:** We explore the prospects of detecting flavorful lepton number violation at the Electron-Ion Collider (EIC) through resonant production of heavy neutral leptons (HNLs), resulting in  $e^- p \rightarrow \ell_\alpha^+ + k j + X$ , where  $\alpha \in \{e, \mu, \tau\}$  and  $k$  denotes the number of jets. We work in the  $\nu$ SMEFT framework of the Standard Model Effective Field Theory augmented with  $n$  singlet HNLs, one of which is in the mass range 10 – 100 GeV, within kinematic reach of the EIC. To explore the EIC sensitivity, we focus on the HNL production mechanism induced by mixing with light neutrinos. We study kinematic distributions for signal and backgrounds, including hadronization and detector effects, and suggest a set of cuts to minimize backgrounds. In the mass range considered, we find that the EIC with muon detection capabilities and an integrated luminosity of 100 fb<sup>-1</sup> can reach sensitivities comparable to the strongest direct (LHC) and indirect constraints, and is especially relevant in the  $\nu$ SMEFT framework beyond dimension four. Our study motivates further assessment of muon detection capabilities at the EIC and  $\tau$  hadronic reconstruction, as well as a more general theoretical analysis involving production mechanisms mediated by higher-dimensional operators in the effective theory.

---

## Contents

<b>1</b>	<b>Introduction</b>	<b>1</b>
<b>2</b>	<b>Theoretical setup</b>	<b>2</b>
<b>3</b>	<b>EIC analysis</b>	<b>5</b>
3.1	Signal	6
3.2	Background	7
3.3	Sensitivity	8
<b>4</b>	<b>Phenomenology</b>	<b>12</b>
4.1	( $\nu$ )SMEFT scenario	14
4.2	Restricted 3 + 1 scenario	18
<b>5</b>	<b>Conclusion and outlook</b>	<b>19</b>
<b>A</b>	<b>Constraints on HNLs from other processes</b>	<b>21</b>
A.1	LEP and LHC constraints	21
A.2	Weak charged-current decays	21
A.3	LFV and LNV decays	22
A.4	Neutrino-less double beta decay	23

---

## 1 Introduction

Probes of lepton number violation (LNV) allow one to explore the possible Majorana origin of neutrino mass and, more generally, physics beyond the Standard Model (BSM) [1, 2]. While neutrinoless double beta ( $0\nu\beta\beta$ ) decay often provides the highest sensitivity to  $\Delta L = 2$  interactions [3], in certain new-physics scenarios other LNV processes, such as lepton and meson decays or high-energy  $ep$  or  $pp$  collisions, can offer competitive sensitivity [2]. In broad brush, a given process can compete with  $0\nu\beta\beta$  decay or can provide complementary information when (i) the LNV process involves particles that can be produced nearly on-shell, thereby overcoming with resonant enhancements the large effective fluxes corresponding to 100's of kilograms of decaying material in  $0\nu\beta\beta$  decay; (ii) the process involves LNV beyond the electron flavor sector. Examples of this second possibility include  $\mu^- \rightarrow e^+$  conversion in nuclei,  $\tau^- \rightarrow \mu^+ \pi^- \pi^-$ ,  $pp \rightarrow \ell_\alpha^\pm \ell_\beta^\pm + X$ ,  $e^- p \rightarrow \ell_\alpha^+ + X$ , with  $\alpha, \beta \in \{\mu, \tau\}$ .

A large class of extensions of the Standard Model (SM) that generate neutrino masses involves new spin-1/2 Majorana fields that are singlets under the SM gauge group [4–8],

called ‘right-handed neutrinos’, ‘sterile neutrinos’, or ‘heavy neutral leptons’ (HNLs) in the literature. Depending on the mass scale associated with the new singlet fields, models with HNLs can be probed in a broad array of processes that conserve or violate lepton number (see Ref. [9] for an overview).

In this study, we will focus on the role that the Electron-Ion-Collider (EIC) [10] can play in probing LNV originating from HNLs in the mass range 10-100 GeV. In this mass range, the leading contribution to LNV signals arises from resonant production of the HNL,  $N$ , in  $e^-p \rightarrow N j + X$  followed by  $N \rightarrow \ell_\alpha^+ + W^*$  ( $\alpha \in \{e, \mu, \tau\}$ ) and  $W^*$  going into hadrons. This channel has previously been studied in the context of HERA [11–13], the LHeC [14–17], and the EIC [18].

Ref. [18] discusses both lepton number conserving and violating effects of HNLs at the EIC. Here we focus on LNV signals and introduce several new elements compared to Ref. [18]:

- First, we perform a more detailed analysis of the LNV signals of HNLs and corresponding backgrounds at the EIC, taking into account parton showering and detector effects.
- Second, we study HNL-induced processes at the EIC that simultaneously violate lepton number and change the flavor of the charged lepton, such as  $e^-p \rightarrow \ell_\alpha^+ + X$ , with  $\alpha \in \{\mu, \tau\}$  (Ref. [18] focused on the  $e^- \rightarrow e^+$  channel), and discuss possible advantages related to smaller SM backgrounds.
- Finally, we compare the sensitivity of the EIC to that of other colliders (LHC, LEP) and low-energy processes, ranging from  $0\nu\beta\beta$  decay to LFV and LNV processes involving  $\mu$  and  $\tau$ , highlighting the discovery potential and complementarity of the EIC in light of these competing searches.

The manuscript is organized as follows: in Section 2 we describe the theoretical framework. In Section 3 we study the expected signal and backgrounds at the EIC, identifying a possible strategy to eliminate the backgrounds. We present our results on the sensitivity of EIC searches in the context of other experimental probes of HNLs in Section 4. Finally, Section 5 summarizes the main results and motivate possible future studies.

## 2 Theoretical setup

Models with HNLs have been extensively studied in the literature (see Ref. [9] and references therein). We explore the EIC sensitivity to HNLs within the following theoretical framework:

- We assume the existence of  $m$  HNLs, of which  $n \leq m$  have masses around or below the electroweak (EW) scale, while the remaining  $m - n$  have masses well above the EW scale.
- We remain agnostic about the underlying model and treat the interactions of the  $n$  HNLs with masses close to or below the EW scale in the  $\nu$ SMEFT [19] framework. The

heavier  $m - n$  HNLs and possibly other heavy particles are integrated out, and their effect is encoded in SMEFT operators (built from SM fields) and  $\nu$ SMEFT operators (involving at least one HNL field) of dimension 5, 6, 7, ..., so that the relevant effective Lagrangian takes the form [20] (we suppress generation indices to avoid clutter)

$$\begin{aligned} \mathcal{L} = & \mathcal{L}_{SM} + \bar{\nu}_R i \not{\partial} \nu_R + \left[ -\frac{1}{2} \bar{\nu}_R^c \bar{M}_R \nu_R - \bar{L} \tilde{H} Y_\nu \nu_R \right. \\ & \left. + \epsilon_{kl} \epsilon_{mn} (L_k^T C^{(5)} C L_m) H_l H_n - \bar{\nu}_R^c \bar{M}_R^{(5)} \nu_R H^\dagger H + C_{\nu B, R} \bar{\nu}_R^c \sigma^{\mu\nu} \nu_R B_{\mu\nu} + \text{h.c.} \right] \\ & + \mathcal{L}_{\nu_L}^{(6)} + \mathcal{L}_{\nu_R}^{(6)} + \mathcal{L}_{\nu_L}^{(7)} + \mathcal{L}_{\nu_R}^{(7)}, \end{aligned} \quad (2.1)$$

where  $\mathcal{L}_{SM}$  is the SM Lagrangian and the three lines in the equation above contain operators of dimension four, five, and six / seven, respectively. We use the notation  $\Psi^c = C \bar{\Psi}^T$  for a spinor field  $\Psi$  in terms of  $C = -C^{-1} = -C^T = -C^\dagger$ , the charge conjugation matrix.  $L = (\nu_L, e_L)^T$  is the left-handed lepton doublet,  $B_{\mu\nu}$  is the fieldstrength of the hypercharge gauge field, while  $\tilde{H} = i\tau_2 H^*$  with  $H$  denoting the Higgs doublet.  $\nu_R$  is a column vector of  $n$  HNLs in the ‘flavor’ basis. The new dimension-three and -four terms involve the complex symmetric  $n \times n$  matrix  $\bar{M}_R$  Majorana mass matrix for the HNLs, and the  $3 \times n$  Yukawa matrix  $Y_\nu$  that couples the HNLs to the SM fields. The dimension-five terms generate Majorana masses for  $\nu_L$  [1] and  $\nu_R$  [21], and a transition magnetic moment for  $\nu_R$ .  $C^{(5)}$ ,  $\bar{M}_R^{(5)}$ , and  $C_{\nu B, R}$  are dimensionful Wilson coefficients containing factors of the EFT breakdown scale  $\Lambda$ . The coefficient of an operator of dimension  $d$  scales as  $C^{(d)} \sim \Lambda^{4-d}$ . The dimension-six and -seven effective Lagrangians  $\mathcal{L}_{\nu_L}^{(6),(7)}$  involving only SM fields were constructed in Refs. [22] and [23], respectively. Similarly, effective Lagrangians  $\mathcal{L}_{\nu_R}^{(6),(7)}$  contain the complete set of dimension-six and -seven operators involving at least one  $\nu_R$  field and were derived in Refs. [19, 20].

- **Mixing:** we work in the basis where the charged leptons  $e_{L,R}^i$  and the quarks  $u_{L,R}^i$ ,  $d_R^i$  are mass eigenstates ( $i = 1, 2, 3$ ). After EW symmetry breaking, this means that  $d_L^{i, \text{gauge}} = V^{ij} d_L^{j, \text{mass}}$ , where  $V$  is the Cabibbo-Kobayashi-Maskawa (CKM) matrix. Up to dimension six, the mass terms of the neutrinos after EW symmetry breaking but before mass-diagonalization take the form,

$$\begin{aligned} \mathcal{L}_m = & -\frac{1}{2} \bar{\mathcal{N}}^c M_\nu \mathcal{N} + \text{H.c.}, \quad M_\nu = \begin{pmatrix} M_L & M_D^* \\ M_D^\dagger & M_R^\dagger \end{pmatrix}, \\ M_L = & -v^2 C^{(5)}, \quad M_R = \bar{M}_R + v^2 \bar{M}_R^{(5)}, \quad M_D = \frac{v}{\sqrt{2}} \left[ Y_\nu - \frac{v^2}{2} C_{L\nu H}^{(6)} \right]. \end{aligned} \quad (2.2)$$

Here  $\mathcal{N} = (\nu_L, \nu_R^c)^T$  making  $M_\nu$  a  $(3+n) \times (3+n)$  symmetric matrix. This matrix can be diagonalized by a transformation involving the unitary matrix  $U$ , given by

$$U^T M_\nu U = m_\nu = \text{diag}(m_1, \dots, m_{3+n}), \quad \text{with } \mathcal{N} = U \mathcal{N}_m. \quad (2.3)$$

The mass eigenstates can be written as  $\nu = \mathcal{N}_m + \mathcal{N}_m^c = \nu^c$ , and we denote the individual mass basis fields as  $\nu^T = (\nu_1, \nu_2, \nu_3, N_4, \dots, N_{3+n})$ . The first three states  $\nu_{1,2,3}$  approximately correspond to active neutrinos with sub-eV masses [24]. We denote the mixing between active, lepton-flavor states  $\alpha \in \{e, \mu, \tau\}$  with (light and heavy) neutrino mass eigenstates  $j \in \{1, \dots, 3+n\}$  by  $U_{\alpha j}$ . From oscillation data,  $|U_{\alpha j}| \sim \mathcal{O}(1)$  for  $j = 1, 2, 3$ , while from various constraints (as described below)  $|U_{\alpha j}| \ll 1$  for  $j \geq 4$ . The charged-current weak vertices relevant for our analysis read

$$\mathcal{L}_{CC} = -\frac{g}{\sqrt{2}} W_\mu^- \sum_{\alpha=e,\mu,\tau} \left( \sum_{i=1}^3 U_{\alpha i} \bar{e}_L^\alpha \gamma^\mu P_L \nu_i + \sum_{j=4}^{3+n} U_{\alpha j} \bar{e}_L^\alpha \gamma^\mu P_L N_j \right). \quad (2.4)$$

Note that the  $3 \times 3$  block  $U_{\alpha i}$  ( $\alpha \in \{e, \mu, \tau\}$  and  $i = 1, 2, 3$ ) of the mixing matrix describing active neutrino mixing is not unitary. In this study, we take a phenomenological approach and consider the masses  $m_j$  and the matrix elements  $U_{\alpha j}$ , with  $j > 3$  and  $\alpha \in \{e, \mu, \tau\}$  as independent parameters, focusing on the effects due to the  $j = 4$  HNL. Finally, for future reference, we also note that the mixing  $U_{si}$  between ‘sterile’ flavors  $s = \{1, \dots, n\}$  and mass eigenstates  $j = \{1, \dots, 3+n\}$  satisfies, by unitarity,  $|U_{sj}| \ll 1$  for  $j = 1, 2, 3$ , while  $|U_{sj}|$  can be  $\mathcal{O}(1)$  for  $j \geq 4$ .

- We consider an effective ‘3 + 1’ setup in which a single HNL,  $N_4$ , with mass  $m_4$ , is kinematically accessible at the EIC, while the remaining  $m - 1$  HNLs are heavier, with masses not far above the electroweak scale.
- To study the reach of the EIC, we focus on the dimension-4 Yukawa interactions and the mass terms in Eq. (2.1). These generate mixing of heavy and light neutrinos, thus inducing the  $W\ell_\alpha N_j$  charged-current vertices proportional to the mixing angle  $U_{\alpha j}$ , given in Eq. (2.4), which in turn control the resonant production of  $N_4$  and its decay, as shown in Fig. 1.

We note that in  $(\nu)$ SMEFT up to dimension seven, there are a handful of additional operators that, in the resonant production of  $N_4$ , can lead to an interference effect with the ‘mixing’ diagrams in Fig. 1, unsuppressed by additional small parameters (charged lepton and quark Yukawa couplings, active-sterile mixing  $U_{\alpha j}$  with  $j = 4, \dots, 3+n$ , and sterile-active mixing  $U_{si}$  with  $i = 1, 2, 3$ ). Their effect can compete with the mixing mechanism if  $U_{\alpha i} \sim (v/\Lambda)^2$  or  $U_{\alpha i} \sim (v/\Lambda)^3$ , which can be realized in models with a relatively low LNV scale. The relevant operators are the dimension-six dipole  $\mathcal{O}_{\nu W} = (\bar{L}\sigma_{\mu\nu}\nu_R)\tau^I \tilde{H}W^{I\mu\nu}$  [20] and the dimension-seven operators  $\mathcal{O}_{NL1} = i\epsilon_{ij}(\bar{\nu}_R^c \gamma_\mu L^i)(D^\mu H)^j (H^\dagger H)$  (which produces a shift to the mixing-induced  $W\ell\nu_R$  vertex) and  $\mathcal{O}_{QNQLH2} = \epsilon_{ij}(\bar{Q}\nu_R)(\bar{Q}^{c,i}L^j)H$  [20]<sup>1</sup>. Other dimension-six and seven operators can also contribute to resonant production, but, as they do not interfere with the mixing mechanism, they do not affect the bounds on  $U_{\alpha 4}$  we will present

<sup>1</sup>In Section 4 we will present a concise discussion of how similar dimension-six and dimension-seven operators affect other observables that are used to constrain the mixing parameters  $U_{\alpha 4}$ .

in Section 4. Here, we focus on the mixing mechanism to explore the relative competitiveness of the EIC, leaving the more general analysis for future work. We expect that the results based on the mixing mechanism, summarized in Section 4.1, will provide a reasonable indication of the competitiveness and complementarity of the EIC with measurements at LEP and the LHC.

In the limit  $n = 1$  and ignoring the higher dimensional ( $\nu$ )SMEFT operators ( $\Lambda \gg v$ ), we obtain a more constrained model, in which many low-energy processes (such as  $0\nu\beta\beta$  decay, lepton-flavor violating processes such as  $\mu \rightarrow e\gamma$ , leptonic and semi-leptonic weak decays of mesons, etc.) indirectly probe the same HNL parameters ( $U_{\ell 4}$  and  $m_4$ ) controlling the EIC signal. Variants of this setup have been studied in detail in Refs. [25–28]. In Appendix A we discuss updates to these analyses relevant for our study. The constraints obtained in the limit  $n = 1$  ignoring ( $\nu$ )SMEFT operators will be presented in Section 4.2.

### 3 EIC analysis

Collider searches for HNLs in  $ep$  collisions have been proposed in the context of HERA [11–13, 29]<sup>2</sup>, the LHeC [14, 15, 31, 32], and more recently the EIC [18]. As in many of them, the event simulation at the matrix-element (ME) level is performed by MadGraph (MadGraph5\_aMC v3.6.2) [33], while the parton shower (PS) and hadronization are handled by Pythia (Pythia8 v8.315) [34]. The ‘SM + HNLs’ model realization in MadGraph was directly taken from the FeynRules (FeynRules v2.3) [35] model database, based on the implementation by the authors of Refs. [36, 37].

From the technical capabilities described in the EIC Yellow Report [38], we select the following operation point for our analysis: center of mass energy  $\sqrt{s} = 141$  GeV ( $E_e \times E_p = 18$  GeV  $\times$  275 GeV), integrated luminosity  $\mathcal{L} = 100$  fb<sup>-1</sup>, and electron polarization  $P_e = 70\%$ . The detector response is managed by Delphes (Delphes3 v3.5.0) [39] using a customized card [40, 41] implementing the specified parameters in the EIC Yellow Report [38]. The same report shows that there are no specific detector capabilities for muons, which are essential for our flavorful analysis. In the spirit of the discussion of a second detector [42–44], we have modified the aforementioned Delphes card to include a future, hypothetical muon detector with the same technical capabilities (efficiency, angular response, energy dependence, etc.) as for electrons.

Multi-jet events generated at fixed-order in QCD may suffer from overestimated cross sections due to large logarithms  $\sigma(e^-p \rightarrow N_4\ell^\pm + k j) \sim \log(\hat{s}/p_{Tj}^2)$  [37], so we impose a set of basic generator-level  $p_{Tj}$  cuts ( $p_{Tj} > 10$  GeV), for both signal and background, to ensure the perturbativity of these logarithms [45]. We additionally implement some complementary generator-level cuts ( $p_{T\ell} > 5$  GeV,  $|\eta_{j,\ell}| < 5$ ,  $\Delta R_{jj,j\ell} > 0.4$ ) and perform parton showering to properly populate the soft region of the  $p_{Tj}$  spectrum<sup>3</sup>. To avoid double-counting between

<sup>2</sup>The H1 Collaboration also has searches for excited neutrino states at HERA [30].

<sup>3</sup>Here,  $\Delta R_{ab} \equiv \sqrt{(\Delta\eta_{ab})^2 + (\Delta\phi_{ab})^2}$  denotes the separation between objects  $a$  and  $b$  in the pseudorapidity–azimuthal angle plane. In particular,  $\Delta R_{jj}$  refers to the jet–jet separation and  $\Delta R_{j\ell}$  to the jet–lepton

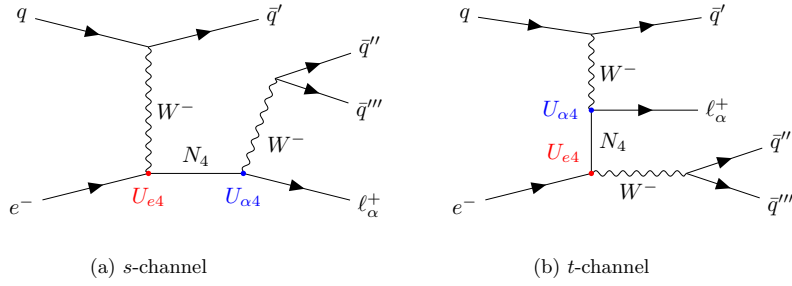


**Figure 1.** Parton-level diagrams for the process  $e^- p \rightarrow \ell_\alpha^+ + k j + X$  ( $\alpha \in \{e, \mu, \tau\}$ ), where  $k$  denotes the number of jets.

matrix-elements and shower emissions, we employ the MLM matching and merging scheme [46], as implemented in MadGraph and Pythia, with `xqcut=10`.

### 3.1 Signal

Based on the experience collected in the existing literature, we study the LNV signal  $e^- p \rightarrow \ell_\alpha^+ + k j + X$  ( $\alpha \in \{e, \mu, \tau\}$ ), where  $k$  denotes the number of jets, mediated by the exchange of a sterile neutrino, as depicted in Fig. 1 at the parton level. While previous strategies have focused solely on  $k = 3$  (e.g., Ref. [18]), a more inclusive approach with  $k = 2$  increases the discovery potential [31]. They both correspond to the same parton-level event in Fig. 1, where the difference occurs at the reconstruction level.

With respect to the two contributions depicted in Fig. 1, the  $s$ -channel dominates for the mass range of interest. Moreover, for the mass range of interest, the width of the sterile neutrino [25, 47–50] is small enough (compared to its mass) to justify the narrow-width approximation (NWA)<sup>4</sup> for a resonant production [52]:

$$\sigma(e^- p \rightarrow \ell_\alpha^+ + k j + X) \approx \sigma(e^- p \rightarrow N_4 j + X) \text{Br}(N_4 \rightarrow \ell_\alpha^+ + k' j) = \frac{|U_{e4} U_{\alpha4}|^2}{U_4^2} \sigma_0(m_4), \quad (3.1)$$

where  $\sigma_0(m_4)$  is a function that depends only on the HNL mass,  $k'$  is the number of jets produced by the decay of  $N_4$ , and we have defined the mixing angle combination

$$U_4 \equiv \sqrt{|U_{e4}|^2 + |U_{\mu4}|^2 + |U_{\tau4}|^2}. \quad (3.2)$$

Note that the width of  $N_4$ ,  $\Gamma_{N_4} \propto U_4^2$ , is dominated by the weak channels  $N_4 \rightarrow Z^{(*)} \nu_i$  ( $i = 1, 2, 3$ ) and  $N_4 \rightarrow W^{\pm(*)} \ell_\alpha^\mp$  ( $\alpha \in \{e, \mu, \tau\}$ ) for  $10 \text{ GeV} \lesssim m_4 < 100 \text{ GeV}$  [50]. Eq. (3.1) effectively shows how the signal cross section can be factorized into a coupling-dependent term and a mass-dependent piece, simplifying the analysis for a parameter scan.

separation.

<sup>4</sup>Recent developments beyond the NWA for large-width scenarios can be found, for instance, in Ref. [51].

The factorization in Eq. (3.1) allows us to study the signal sensitivity in terms of the HNL mass ( $m_4$ ) and the coupling combination  $|U_{e4}U_{\alpha 4}|^2/U_4^2$  for the three different channels ( $\alpha \in \{e, \mu, \tau\}$ ). For the electron channel, namely  $e^-p \rightarrow e^+jj(j)$ , we target an isolated positron in the final state. For both the muon and tau channels, we opted for the reconstruction of a  $\mu^+$ . While the  $\tau$  decay mode into muons has a branching ratio  $\approx 17\%$  [53], it provides a relatively clean environment compared with the hadronic decay modes [54]. Improving the analysis in the hadronic channels could highly impact the EIC reach, but we defer this dedicated study to future work.

In principle, the same strategy could also be applied to the lepton-number conserving (LNC) counterpart of the process for all three lepton-flavor channels, since the production mechanism and resonant kinematics remain unchanged. Particularly, in the LNC case for the electron channel, the corresponding SM backgrounds are significantly larger, substantially reducing the achievable sensitivity. In the muon and  $\tau$  channels, we expect the LNC and LNV channels to have similar sensitivities.

### 3.2 Background

The SM background for LNV searched in  $ep$  collisions has been described in the literature [11–15, 18, 29, 31, 32] and can be categorized in three types:

- **Deep inelastic scattering (DIS)**

In neutral-current DIS (NC-DIS),  $e^-p \rightarrow e^- + X$ , the scattered lepton yields an isolated electron signature, while the multi-jet component originates from QCD radiation. In the electron channel, an important reducible background arises from charge misidentification, whereby isolated electrons are reconstructed as positrons, primarily due to hard bremsstrahlung in the tracker material<sup>5</sup>. Following analogous studies in the LHC context [55–57, 59], we model this contribution through an electron charge-misidentification probability  $P_{\text{misID}}$ . While a realistic treatment would require a detector-dependent parametrization (*e.g.*, angular and energy dependence), we adopt a constant benchmark value  $P_{\text{misID}} = 10^{-3}$  [18, 57], which is conservative and likely underestimates the achievable sensitivity once a full detector study is performed.

In the muon and  $\tau$  channels, NC-DIS constitutes an irreducible background, as hadronization can produce secondary decays yielding muons and  $\tau$  leptons. We simulate multi-jet DIS samples by matching and merging matrix-element configurations with one, two, and three parton-level jets using MadGraph interfaced with Pythia.

Our simulations show that NC-DIS is one of the main background components across all lepton-flavor channels, in agreement with the results of Ref. [18] for the electron/positron channel.

---

<sup>5</sup>The so-called trident process  $e^- \rightarrow e^- \gamma^* \rightarrow e^- e^+ e^-$  [55–57]. Since the bremsstrahlung rate scales approximately as  $m_\ell^{-4}$  [58], this effect is negligible for muons.

In charged-current DIS (CC-DIS),  $e^-p \rightarrow \nu_e + X$ , the absence of a prompt charged lepton at the hard-scattering level does not preclude lepton production at later stages. Hadronization and subsequent hadron decays can generate secondary electrons, muons, and  $\tau$  leptons, thereby populating all three signal channels. As a result, CC-DIS constitutes an irreducible background for the electron, muon, and  $\tau$  channels. Our simulations indicate that CC-DIS represents a sizable contribution to the total background.

- **Heavy quark production**

Boson-gluon fusion into a pair of heavy quarks ( $e^-p \rightarrow e^- + \bar{Q}Q + X$ ) may contribute as a background source due to the presence of isolated leptons in the decay of the heavy quarks. The scattered electron is not reconstructed, either because it is collimated along the beamline or because it participates in a charged-current interaction producing a neutrino and a  $W$  boson<sup>6</sup>. We simulated heavy-quark-pair production (matched and merged up to one extra jet) for  $b$ -quarks, keeping the default MadGraph settings to treat  $\{u, d, s, c\}$  as light quark flavors. Dealing with charm quarks also as heavy flavors, although highly motivated in the context of the EIC [40, 60], goes beyond the scope of this work.

We find that this background is sizable for all lepton-flavor channels. Ref. [18] did not include this channel in their background estimation for the electron/positron channel. Since the analysis of Ref. [18] was carried out at the parton level, *i.e.*, neglecting hadronization effects, the omission of heavy-quark-pair production may be attributable to its incompatibility with this level of description.

- **$W$  boson production**

Similar to the previous case, the production of a  $W$  boson and its subsequent decay will contribute with either jets or leptons. The main contributions to this background source come from  $e^-p \rightarrow \nu_e + W^\pm + X$  and  $\gamma p \rightarrow W^\pm + X$ , where the photon is radiated by the incoming electron. Subsequent  $W$  boson decays are responsible for the presence of isolated leptons. In MadGraph, the photoproduction is simulated using the Weizsäcker-Williams approximation [61].

Our results indicate that this background class is negligible compared to the previous two, in agreement with the findings of Ref. [18]. We therefore neglect this contribution in the subsequent analysis.

### 3.3 Sensitivity

To evaluate the EIC sensitivity to HNLs, we perform a proof-of-principle cut-based analysis. Although a more sophisticated approach involving multivariate analysis techniques or artificial intelligence/machine learning (AI/ML) could yield better performance, we emphasize the goal of this work is to motivate future developments (both theoretical and experimental) to improve the EIC’s sensitivity for BSM physics.

---

<sup>6</sup>In principle, charge misidentification could also play a role, but the effect is negligible.

We generated  $10^7 - 10^8$  events for each of the relevant background types (heavy-quark production, CC-DIS, and NC-DIS), and  $10^6$  events for the signal process  $e^-p \rightarrow \ell_\alpha^+ + k j + X$  ( $\alpha \in \{e, \mu, \tau\}$ ) with fixed HNL masses  $m_4 = \{10, 25, 40, 55, 70, 85, 100\}$  GeV. To identify the relevant signal-like events, we impose a preliminary set of signal selection cuts listed in Box I.

**Box I. Signal selection cut (Cut-SS)**

- Exactly two or three jets:  $N_j = 2, 3$ .
- Exactly one positively charged lepton:
  - For the electron channel,  $N_{e^+} = 1$ .
  - For the muon and tau channels,  $N_{\mu^+} = 1$ , with an electron veto applied.
  - For backgrounds involving charge misidentification, we select one electron ( $N_{e^-} = 1$ ) and weight the events by the charge misidentification probability  $P_{\text{misID}}$ .
- Jet–jet and jet–lepton isolation,  $\Delta R_{jj, j\ell} > 0.4$ , and detector acceptance requirement  $|\eta_{j,\ell}| < 5$ .

To identify a feasible set of kinematic cuts that isolate signal from background, we analyzed the distributions of several common kinematic variables after applying the signal selection criteria (Cut-SS) in Box I. The most relevant results are displayed in Figs. 2, 3, and 4 for the electron, muon, and  $\tau$  channels, respectively. For many kinematic variables (for example, azimuthal angle or pseudorapidity distributions for jets and leptons), there is significant overlap between the background and signal. The transverse momentum of the final-state lepton,  $p_{T\ell}$ , the missing transverse energy,  $E_T^{\text{miss}}$ , and the transverse momenta of the leading jets,  $p_{Tj}^{(i)}$  ( $i = 1, 2, 3$ ), provide good discrimination between signal and background. We therefore characterize the jet activity through  $H_T \equiv \sum_i p_{Tj}^{(i)}$ , the scalar sum of the jet transverse momenta. We also include the reconstructed invariant mass  $M_{\ell jj}$  of the lepton and any pair of jets, which is commonly used in searches involving direct production [11–15, 18, 29, 31, 32].

Our results differ from similar electron-channel distributions reported in Ref. [18] due to two main effects. First, the generator-level cuts imposed in our analysis (introduced to ensure the stability and reliability of the matrix-element calculation) are more restrictive than those applied in Ref. [18]. These tighter requirements already modify the event kinematics at the parton level, particularly in the soft and low-mass regions. Second, our simulation includes parton showering and hadronization, which further distorts the kinematic distributions of jets and leptons, whereas Ref. [18] is based on a purely parton-level study. The combined impact of these effects is most clearly visible in the  $M_{\ell jj}$  distributions shown in Fig. 2. Although resonant structures around  $M_{\ell jj} \sim m_4$  are present for all HNL masses considered, the peaks are significantly broadened relative to the parton-level results of Ref. [18]. Consequently, the

mass-window variable  $\Delta M^{\min} \equiv \min_{a,b}(|M_{\ell j_a j_b} - m_4|)$ , which was adopted in Ref. [18], does not provide the same level of discrimination in our setup. For this reason, we do not include  $\Delta M^{\min}$  among the observables used in our analysis.

As shown in Figs. 2–4, requiring  $H_T \gtrsim 50$  GeV provides strong separation between signal and background, particularly in the muon and  $\tau$  channels. In addition, imposing  $p_{T\ell} \gtrsim 5$  GeV efficiently suppresses the heavy-quark production background in all channels and further reduces the NC-DIS contribution in the muon and  $\tau$  modes. In the  $\tau$  channel, the  $p_{T\ell}$  distribution of the signal is shifted toward lower values, since the isolated muon arises from the decay of a  $\tau$ , leading to a softer transverse-momentum spectrum. Hadronization effects and detector resolution induce a substantial overlap between the  $E_T^{\text{miss}}$  spectra of signal and background. An exception arises in the  $\tau$  channel, where additional neutrinos from leptonic  $\tau$  decays broaden the signal  $E_T^{\text{miss}}$  distribution, motivating the requirement  $E_T^{\text{miss}} \gtrsim 5$  GeV. The CC-DIS background also displays a broader and more forward  $E_T^{\text{miss}}$  distribution, which could in principle motivate additional upper bounds,  $E_T^{\text{miss}} \lesssim 20$  GeV and  $\eta_{E_T^{\text{miss}}} \lesssim -2$ . In practice, however, the existing  $H_T$  and  $p_{T\ell}$  requirements already suppress the CC-DIS contribution efficiently, rendering further cuts redundant.

Consolidating these results, we propose a set of kinematic cuts for each lepton-flavor channel, defined explicitly in Boxes II–IV. Table 1 summarizes their performance for two representative HNL mass benchmarks, illustrating how the successive selections suppress the dominant backgrounds while retaining signal efficiency. Entries expressed as  $\mathcal{O}(\cdot)$  indicate that no simulated events survive the corresponding cut combination; the quoted value reflects the upper bound obtained from a single event with unit weight in the Monte Carlo sample.

#### Box II. Electron channel cuts (Cut- $e$ )

- All the requirements from Cut-SS in Box I.
- $p_{T_e} > 5$  GeV and  $H_T > 50$  GeV.

#### Box III. Muon channel cuts (Cut- $\mu$ )

- All the requirements from Cut-SS in Box I.
- $p_{T_\mu} > 5$  GeV and  $H_T > 50$  GeV.

#### Box IV. $\tau$ channel cuts (Cut- $\tau$ )

- All the requirements from Cut-SS in Box I.
- $p_{T_\mu} > 5$  GeV,  $H_T > 50$  GeV, and  $E_T^{\text{miss}} > 5$  GeV.

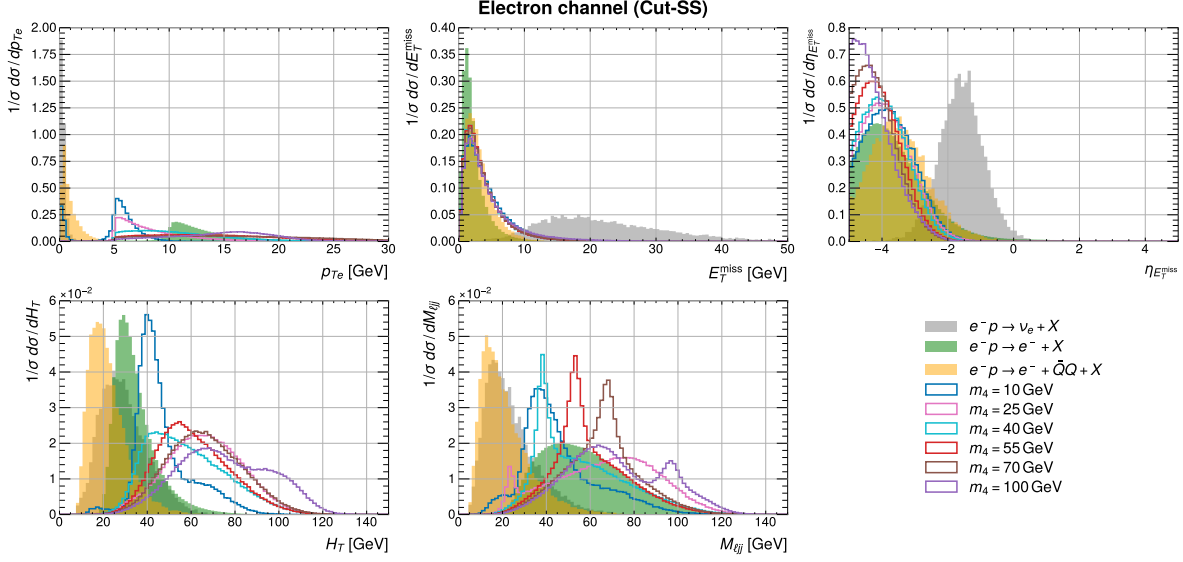


**Figure 2.** Kinematic distributions for the electron channel  $e^-p \rightarrow e^+jj(j)$  after imposing the signal selection cuts (Cut-SS) in Box I. Background contributions are shown as filled histograms, while representative HNL mass benchmarks are displayed as solid lines.

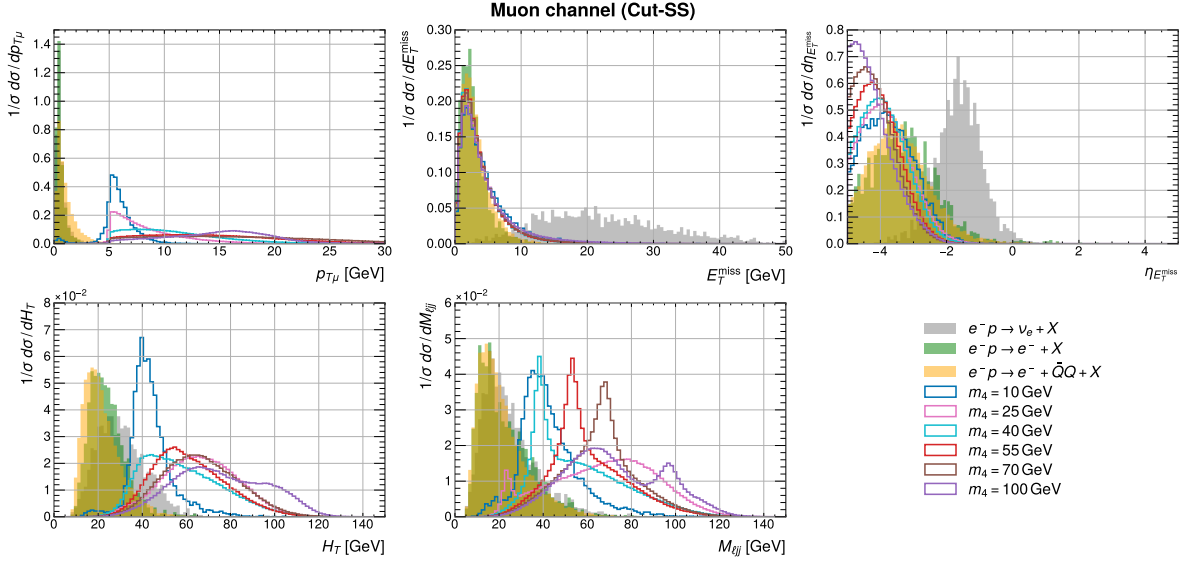


**Figure 3.** Kinematic distributions for the muon channel  $e^-p \rightarrow \mu^+jj(j)$ , with the same conventions as in Fig. 2.

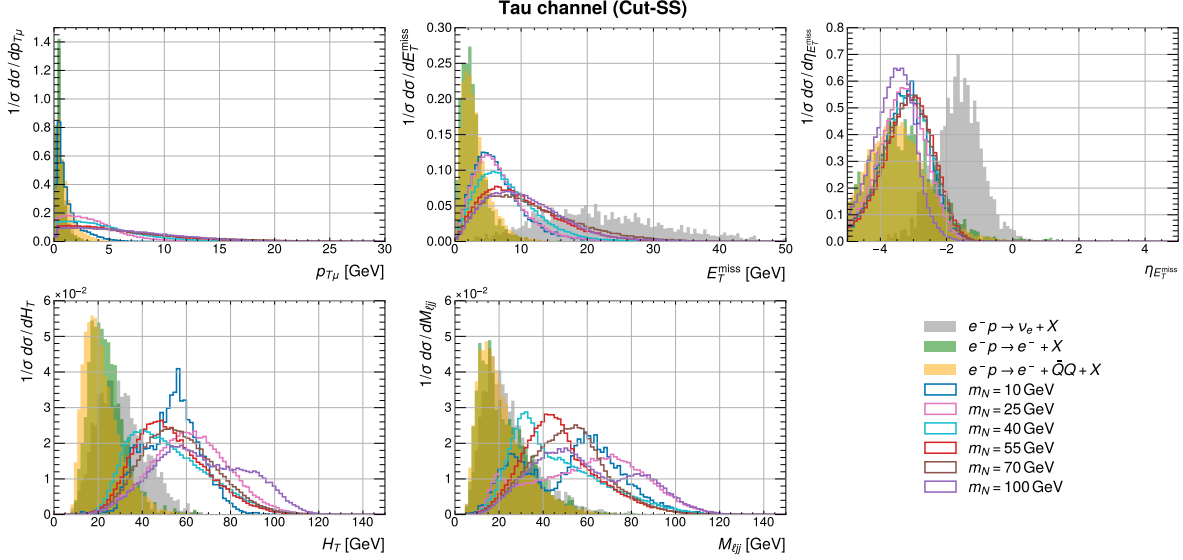


**Figure 4.** Kinematic distributions for the  $\tau$  channel  $e^-p \rightarrow \tau^+ jj(j)$ , with the same conventions as in Fig. 2.

## 4 Phenomenology

In this section, we discuss the impact of HNL searches at the EIC in the context of other HNL probes. In the mass region of interest ( $m_4 \sim 10\text{-}100$  GeV), the strongest constraints on HNL couplings arise from [25–28, 62, 63] (i) collider searches at the LHC; (ii)  $Z$  decays at LEP; (iii) weak decays of mesons; (iv) LFV and (to a lesser extent) LNV decays of leptons and mesons; (v)  $0\nu\beta\beta$  decay. In the context of 3+1 models without inclusion of  $\nu$ SMEFT operators, these processes are studied together, as they all constrain the HNL mixing parameters  $U_{\alpha 4}$  and  $m_4$ .

As discussed in Section 2, here we consider a more general setup that includes ( $\nu$ )SMEFT operators up to dimension seven. In this framework the EIC resonant cross section  $e^-p \rightarrow \ell_\beta^+ + X$  and the corresponding ‘crossed’ process at the LHC,  $pp \rightarrow e^\pm \ell_\beta^\pm + X$ , probe the same couplings, though not necessarily with the same relative weight, given the different energies involved. Here, we have considered only the mixing-induced production and decay. On the other hand, probes in classes (ii) to (v) above are sensitive to different combinations of mixing angles and ( $\nu$ )SMEFT Wilson Coefficients compared to the EIC resonant cross section.

We summarize here the ( $\nu$ )SMEFT contributions to probes (ii) to (v) that can interfere with the mixing-induced contributions, possibly diluting the corresponding indirect bounds on  $|U_{\alpha 4} U_{\beta 4}|$ . As in Section 2, we focus on effects that are suppressed only by the ( $\nu$ )SMEFT expansion parameter  $(v/\Lambda)^n$  ( $n = 2, 3$ ), without additional suppression due to ‘wrong chirality’ in the neutrino, charged leptons, and quarks. (ii) The process  $Z \rightarrow N_4 \nu_i$  ( $i = 1, 2, 3$ ) receives contributions from a linear combination of the dimension-six operators  $\mathcal{O}_{\nu B} = (\bar{L}\sigma_{\mu\nu}\nu_R)\tilde{H}B^{\mu\nu}$  [20] and  $\mathcal{O}_{\nu W} = (\bar{L}\sigma_{\mu\nu}\nu_R)\tau^I\tilde{H}W^{I\mu\nu}$  [20], as well as the oper-

Lepton flavor channel	Background			Mass benchmark		
	NC-DIS	CC-DIS	Heavy-quark	$m_4 = 10 \text{ GeV}$	$m_4 = 70 \text{ GeV}$	
	[pb]	[pb]	[pb]	[pb]	[pb]	
$e$	ME+PS	$2.37 \times 10^0$	$2.36 \times 10^1$	$3.32 \times 10^1$	$1.01 \times 10^{-2}$	$7.47 \times 10^{-2}$
	Cut-SS	$9.15 \times 10^{-2}$	$5.35 \times 10^{-3}$	$6.50 \times 10^{-2}$	$7.99 \times 10^{-5}$	$3.08 \times 10^{-2}$
	Cut- $e$	$7.28 \times 10^{-3}$	$8.91 \times 10^{-7}$	$3.54 \times 10^{-6}$	$7.94 \times 10^{-6}$	$2.55 \times 10^{-2}$
$\mu$	ME+PS	$2.37 \times 10^3$	$2.36 \times 10^1$	$3.32 \times 10^1$	$9.90 \times 10^{-3}$	$7.47 \times 10^{-2}$
	Cut-SS	$5.56 \times 10^{-2}$	$8.45 \times 10^{-4}$	$6.65 \times 10^{-2}$	$7.64 \times 10^{-5}$	$3.77 \times 10^{-2}$
	Cut- $\mu$	$< \mathcal{O}(10^{-5})$	$< \mathcal{O}(10^{-7})$	$1.07 \times 10^{-5}$	$9.16 \times 10^{-6}$	$3.13 \times 10^{-2}$
$\tau$	ME+PS	$2.37 \times 10^3$	$2.36 \times 10^1$	$3.32 \times 10^1$	$9.93 \times 10^{-3}$	$7.47 \times 10^{-2}$
	Cut-SS	$5.56 \times 10^{-2}$	$8.45 \times 10^{-4}$	$6.65 \times 10^{-2}$	$7.58 \times 10^{-5}$	$6.13 \times 10^{-3}$
	Cut- $\tau$	$< \mathcal{O}(10^{-5})$	$< \mathcal{O}(10^{-7})$	$3.55 \times 10^{-6}$	$5.95 \times 10^{-8}$	$1.95 \times 10^{-3}$

**Table 1.** Cut-flow table for the dominant SM backgrounds and the LNV signal in the three lepton-flavor channels. All entries are cross sections in pb. The collider setup assumes  $\sqrt{s} = 141 \text{ GeV}$  ( $E_e \times E_p = 18 \text{ GeV} \times 275 \text{ GeV}$ ) and electron polarization  $P_e = 70\%$ . The rows labeled ME+PS correspond to matched matrix-element plus parton-shower simulations prior to any kinematic selections. Cut-SS denotes the signal selection requirements of Box I, while Cut- $e$ , Cut- $\mu$ , and Cut- $\tau$  refer to the channel-dependent cuts defined in Boxes II–IV. The signal benchmarks correspond to  $m_4 = 10 \text{ GeV}$  and  $m_4 = 70 \text{ GeV}$  with  $|U_{e4}| = |U_{\mu4}| = |U_{\tau4}| = 1$ . When applicable (*e.g.*, in the electron channel), the results have been weighted by a charge-misidentification probability  $P_{\text{misID}} = 10^{-3}$ . Entries expressed as  $\mathcal{O}(\cdot)$  indicate that no simulated events survive the corresponding cut combination; the quoted value reflects the upper bound obtained from a single event with unit weight in the Monte Carlo sample.

ators  $\mathcal{O}_{NL1} = i\epsilon_{ij}(\bar{\nu}_R^c \gamma_\mu L^i)(D^\mu H)^j(H^\dagger H)$  and  $\mathcal{O}_{NL2} = \epsilon_{ij}(\bar{\nu}_R^c \gamma_\mu L^i)H^j(iH^\dagger \overleftrightarrow{D}_\mu H)$  [20] arising at dimension seven. (iii) Weak decays  $d_j \rightarrow u_i \ell_\alpha \bar{\nu}_\alpha$  are affected by heavy-light neutrino mixing and by the dimension-six operators in SMEFT, resulting in effective vertices  $G_F V_{u_i d_j} \times [1 + (1/2)(|U_{e4}|^2 + |U_{\mu4}|^2 - |U_{\alpha4}|^2) + \epsilon_L^{(\alpha)}]$ , where  $\epsilon_L^{(\alpha)}$  denotes a linear combination of dimension-six SMEFT couplings [64, 65]. (iv) LFV decays of charged leptons and mesons can receive interfering contributions from  $N_5 - N_{3+n}$  as well as from dimension-six SMEFT operators. (v) Similarly, in addition to the combination  $U_{e4}^2/m_4$ ,  $0\nu\beta\beta$  decay receives interfering contributions from  $N_5 - N_{3+n}$  and from dimension-seven SMEFT operators [23, 66].

Based on the above discussion, we present our results as follows:

- First, we show the EIC sensitivity to the combination  $|U_{\alpha4}U_{\beta4}|^2/(|U_{e4}|^2 + |U_{\mu4}|^2 + |U_{\tau4}|^2)$

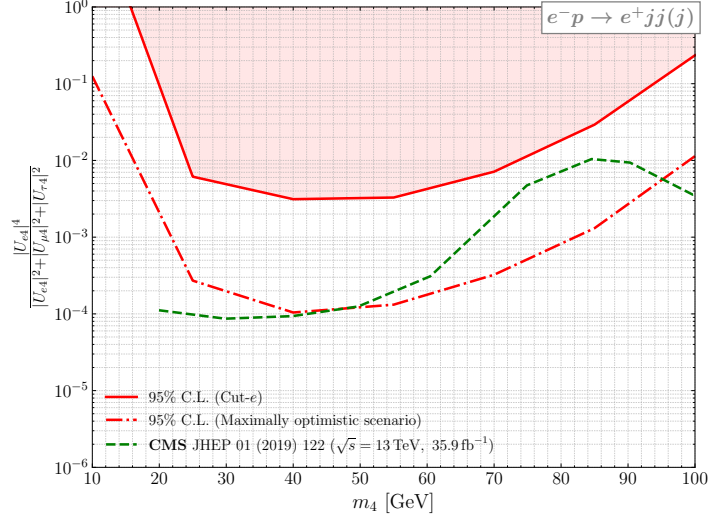


**Figure 5.** Expected 95% C.L. exclusion limits from the electron channel  $e^-p \rightarrow e^+jj(j)$  at the EIC with  $\sqrt{s} = 141$  GeV ( $E_e \times E_p = 18$  GeV  $\times$  275 GeV), integrated luminosity  $\mathcal{L} = 100$  fb $^{-1}$ , and electron polarization  $P_e = 70\%$ . A charge-misidentification probability  $P_{\text{misID}} = 10^{-3}$  is assumed. The solid red curve shows the limits obtained after applying the kinematic cuts (Cut- $e$ ) of Box II, while the red dot-dashed curve corresponds to a maximally optimistic scenario with complete background rejection and perfect signal reconstruction (see text for details). The dashed green curve corresponds to a CMS analysis at the LHC probing the same coupling combination through resonant production in  $\ell +$  jets final states, using a comparable analysis strategy [67].

as a function of  $m_4$ , along with a direct comparison to existing constraints from the LHC. This assumes that  $(\nu)$ SMEFT operators are present and dilute the constraints on the mixing angles from the indirect probes (ii)-(v) above.

- We subsequently discuss the more restrictive model in which  $n = 1$  and the  $(\nu)$ SMEFT operators are ignored, showing all constraints, including the ones from probes (ii)-(v), in the  $|U_{\alpha 4}U_{\beta 4}| - m_4$  plane. For the latter analysis, we rely in part on recent global analyses [25–28, 62, 63], with updates provided in Appendix A, which include an improved evaluation of the strongest bound on  $|U_{e4}|$ , arising from  $0\nu\beta\beta$  decay.

#### 4.1 $(\nu)$ SMEFT scenario

From the kinematic requirements summarized in Boxes II–IV, we obtain the expected signal and background number of events,  $N_s$  and  $N_b$ , respectively, for each lepton-flavor channel. These event counts are then used to derive exclusion limits on the coupling strength  $|U_{e4}U_{\alpha 4}|^2/U_4^2$  ( $\alpha \in \{e, \mu, \tau\}$ ) as a function of the HNL mass  $m_4$ .

Assuming the background prediction is known with negligible uncertainty, we compute the upper bound on the signal contribution using a Bayesian approach following Ref. [68]. For an observed number of events  $N_{\text{obs}}$  and expected background  $N_b$ , the  $(1 - \alpha_{\text{CL}})$  credibility

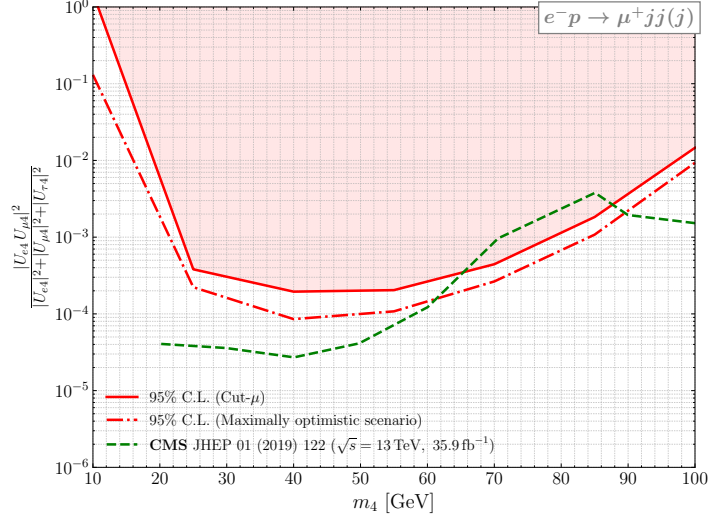


**Figure 6.** Expected 95% C.L. exclusion limits from the muon channel  $e^-p \rightarrow \mu^+ jj(j)$ , assuming an integrated luminosity  $\mathcal{L} = 100 \text{ fb}^{-1}$ , and following the same conventions as in Fig. 5. The dashed green curve corresponds to a CMS analysis at the LHC probing the same coupling combination through resonant production in  $\ell + \text{jets}$  final states, using a comparable analysis strategy [67].

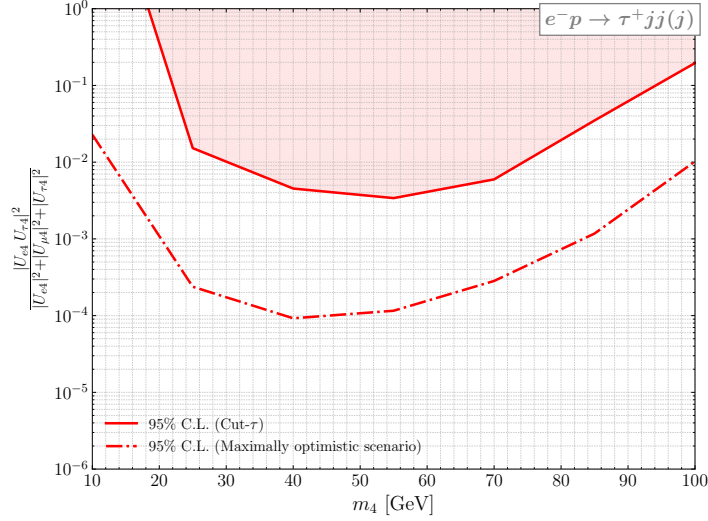


**Figure 7.** Expected 95% C.L. exclusion limits from the  $\tau$  channel  $e^-p \rightarrow \tau^+ jj(j)$ , assuming an integrated luminosity  $\mathcal{L} = 100 \text{ fb}^{-1}$ , and following the same conventions as in Fig. 5.

upper limit on  $N_s$  is obtained from

$$1 - \alpha_{\text{CL}} = 1 - \frac{\Gamma(1 + N_{\text{obs}}, N_b + N_s)}{\Gamma(1 + N_{\text{obs}}, N_b)}, \quad (4.1)$$

where  $\Gamma(a, x)$  is the incomplete gamma function. In the sensitivity projections, we assume the background-only hypothesis,  $N_{\text{obs}} = N_b$  [54], thereby extracting the expected upper limit on  $N_s$  and translating it into a bound on the coupling strength. The 95% C.L. exclusion

curves for each lepton-flavor channel are presented in Figs. 5–7. The results correspond to an EIC setup with  $\sqrt{s} = 141 \text{ GeV}$  ( $18 \text{ GeV} \times 275 \text{ GeV}$ ),  $\mathcal{L} = 100 \text{ fb}^{-1}$ , and  $P_e = 70\%$ . A charge-misidentification probability  $P_{\text{misID}} = 10^{-3}$  is assumed.

For each lepton-flavor channel, we present the 95% C.L. exclusion limits under two benchmark scenarios. The solid red curves correspond to the expected sensitivity obtained after applying the kinematic requirements (Cut- $e$ , Cut- $\mu$ , and Cut- $\tau$ ) defined in Boxes II–IV. As indicated by the cut-flow results in Table 1, the residual background contribution remains non-negligible for the  $e$  case, while, for the assumed luminosity, it is reduced to one (less than one) event in the  $\mu$  ( $\tau$ ) case. In addition, we consider a ‘maximally optimistic scenario’, defined by the assumptions of complete background rejection and perfect signal reconstruction. The corresponding limits are obtained by setting  $N_{\text{obs}} = N_b = 0$  in Eq. (4.1) and retaining all signal events passing the signal selection criteria (Cut-SS) in Box I. For the  $\tau$  channel, this scenario implicitly assumes full  $\tau$  reconstruction efficiency, including hadronic decay modes, thereby providing an estimate of the highest sensitivity achievable under ideal detector performance.

As shown in Figs. 5–7, the three lepton-flavor channels exhibit comparable sensitivity across the HNL mass range. The reach of the EIC deteriorates for  $m_4 \gtrsim 100 \text{ GeV}$ , reflecting the kinematic limitations imposed by the center-of-mass energy. A similar degradation occurs for  $m_4 \lesssim 10 \text{ GeV}$ , where the generator-level  $pt_j$  requirements reduce the efficiency for very light HNLs produced near threshold. Since the signal proceeds through resonant production, the visible jet kinematics become increasingly soft at low masses, leading to a loss of acceptance. In the electron channel  $e^-p \rightarrow e^+jj(j)$ , Fig. 5, the presence of residual background (predominantly NC-DIS) reduces the sensitivity by about one order of magnitude compared to the maximally optimistic scenario. A smaller charge-misidentification probability would reduce this gap, highlighting the importance of a realistic assessment of  $P_{\text{misID}}$  for LNV searches at the EIC. Conversely, Fig. 6 indicates that the muon channel  $e^-p \rightarrow \mu^+jj(j)$  benefits from a particularly clean experimental signature, underscoring the importance of dedicated muon identification capabilities at the EIC [42–44]. Note that Figs. 5 and 6 also display the existing CMS constraint from a resonant HNL search in  $\ell + \text{jets}$  final states at the LHC [67]. This analysis probes the same coupling combination using a comparable resonant production topology and analysis strategy in a similar mass range, allowing for a direct comparison between the projected EIC sensitivity and current LHC bounds. Other resonant searches at the LHC (*e.g.*, Refs. [69–72]) either explore different mass regimes, production mechanisms, or constrain alternative combinations of mixing parameters, highlighting the complementarity of the EIC program. Finally, Fig. 7 presents the projected sensitivity in the  $\tau$  channel  $e^-p \rightarrow \tau^+jj(j)$ . Although the analysis also considers the muon final state, the corresponding limits do not follow a simple rescaling by the relevant branching ratios. This is because the signal kinematics differ significantly between the two channels, as reflected in the distinct distributions shown in Figs. 3 and 4. A substantial improvement is observed in the maximally optimistic scenario, where hadronic  $\tau$  decay modes are assumed to be fully reconstructed in addition to the leptonic ones. This highlights the strong impact that an

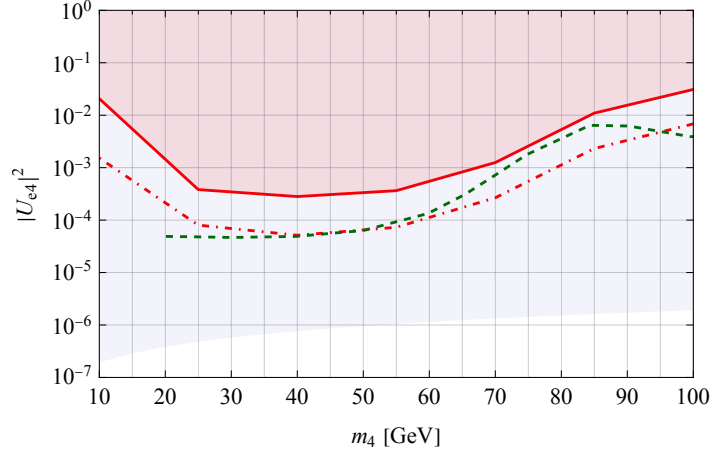


**Figure 8.** The red (green) lines show the expected 95% C.L. exclusion limits on  $|U_{e4}|^2$  from the EIC analysis (the current LHC bound), which have been converted from the bounds depicted in Fig. 5 by setting  $U_4$  to its upper limit, which provides an upper bound on the EIC sensitivity. In the restricted  $3 + 1$  scenario, the shaded blue region is excluded by other constraints, dominated in this case by a combination of  $0\nu\beta\beta$  decay and tritium  $\beta$  decay.

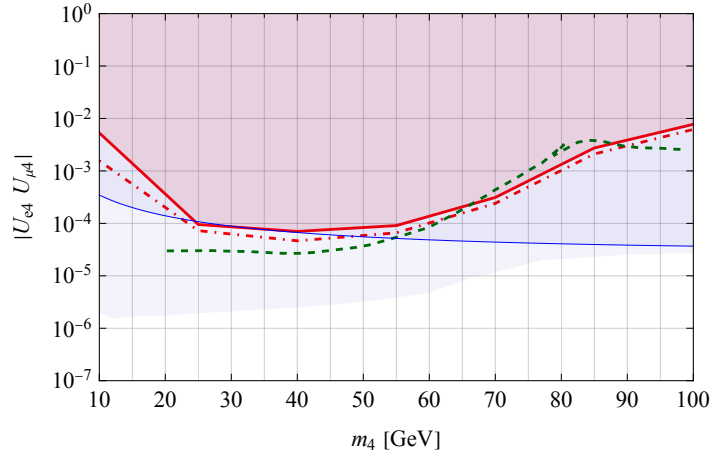


**Figure 9.** The red (green) lines show the expected 95% C.L. exclusion limits on  $|U_{e4}U_{\mu4}|$  from the EIC analysis (the current LHC bound), which have been converted from the bounds depicted in Fig. 6 by setting  $U_4$  to its upper limit, which provides an upper bound on the EIC sensitivity. The shaded blue region is excluded by combining constraints on  $|U_{e4}|$  (dominated by a combination of  $0\nu\beta\beta$  decay and tritium  $\beta$  decay) and  $|U_{\mu4}|$  (dominated by LEP and LHC searches), while the thin solid line shows the constraint from  $\mu \rightarrow e$  conversion, which directly probes the combination  $|U_{e4}U_{\mu4}|$ .

efficient and dedicated  $\tau$  reconstruction program could have on the sensitivity to LNV signals at the EIC.

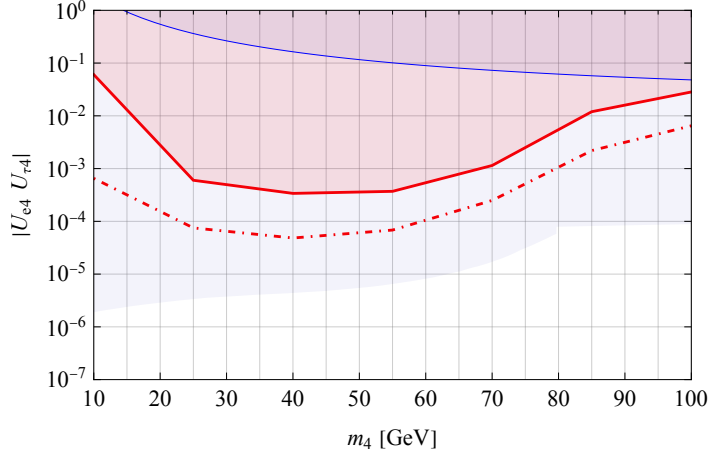


**Figure 10.** The red lines show the expected 95% C.L. exclusion limits on  $|U_{e4}U_{\tau 4}|$  from the EIC analysis, which have been converted from the bounds depicted in Fig. 7 by setting  $U_4$  to its upper limit, which provides an upper bound on the EIC sensitivity. The shaded blue region is excluded by combining constraints on  $|U_{e4}|$  (dominated by a combination of  $0\nu\beta\beta$  decay and tritium  $\beta$  decay) and  $|U_{\tau 4}|$  (dominated by  $Z$  decays), while the thin solid line shows the constraint from  $\tau \rightarrow e\gamma$ , which directly probes the combination  $|U_{e4}U_{\tau 4}|$ .

## 4.2 Restricted 3 + 1 scenario

In the restricted case, for fixed  $m_4$ , the relevant observables can be parameterized in terms of the following combinations of  $U_{e4}, U_{\mu 4}, U_{\tau 4}$ ,

$$|U_{e4}|^2, \quad |U_{e4}U_{\mu 4}|, \quad |U_{e4}U_{\tau 4}|, \quad |U_{\mu 4}U_{\tau 4}|, \quad U_4. \quad (4.2)$$

In order to directly compare EIC (and LHC) constraints to the other probes, we plot (products of) the mixing angles versus  $m_4$  for fixed values of  $U_4$ , set to the maximum allowed value. To obtain the latter, we combine the bounds on the individual  $U_{\alpha 4}$ . For  $\alpha = e$ , the limit is dominated by  $0\nu\beta\beta$  decay combined with measurements of tritium  $\beta$  decays, as discussed in Appendix A.4. For  $\alpha = \mu$  the bounds are set by the combination of ATLAS [72] and CMS [71] constraints on  $|U_{\mu 4}|^4/U_4^2$  and the LEP search for  $Z$  decays into a HNL and a light neutrino [73] for most of the mass range, while weak decays dominate for  $m_4 \gtrsim m_W$ , see Appendices A.2 and A.1, respectively. Instead, the LHC searches do not play a role in the case of  $\alpha = \tau$ . As a result, the combined constraint on  $U_4$  is determined mostly by  $Z$  decays up to  $m_4 \simeq m_W$ , above which the limit from weak decays takes over. To show the EIC limits on the combinations  $|U_{e4}U_{\alpha 4}|$ , we multiply the constraints shown in Figs. 5-7, by the bound on  $U_4^2$  and take the square root. We emphasize that this gives rise to a conservative constraint, since we used the upper limit on  $U_4$ .

We plot the resulting 95% C.L. limits in Figs. 8 - 10. The EIC bounds are again shown in red, while the limits from other probes are depicted by the blue shaded regions. These are obtained by combining the most stringent limits on the separate mixing-matrix elements,  $U_{\alpha 4}$ , similar to the procedure for  $U_4$  mentioned above. In addition, the solid thin lines in Figs.

9 and 10 show the limits from  $\mu \rightarrow e$  conversion and  $\tau \rightarrow e\gamma$  that directly probe the flavor-changing combinations,  $|U_{e4}U_{\mu4}|$  and  $|U_{e4}U_{\tau4}|$ , respectively (see Appendix A.3 for details). In all cases, at face value the other probes tend to be more sensitive than the projected upper bound from the EIC by an order of magnitude or more. On the other hand, the latter have a comparable sensitivity to  $\mu \rightarrow e$  conversion in the range  $m_4 = (20 - 60)$  GeV and are more sensitive than  $\tau \rightarrow e\gamma$ .

## 5 Conclusion and outlook

The search for phenomena that violate the conservation of lepton number is well motivated, and a non-zero signal would have implications for the understanding of neutrino mass generation and broader BSM physics, including the generation of the cosmic baryon asymmetry. In this manuscript, we have explored the prospects of detecting LNV at the EIC through resonant production of a heavy Majorana neutral lepton ( $N_4$ ),  $e^-p \rightarrow N_4 + X$ , followed by  $N_4 \rightarrow \ell_\alpha^+ + W^*$  ( $\alpha \in \{e, \mu, \tau\}$ ), with the  $W$  decaying into hadrons, resulting in lepton number and possibly lepton flavor violating signatures  $e^-p \rightarrow \ell_\alpha^+ + k j + X$  where  $k = 2, 3$  denotes the number of jets.

We work in the theoretical framework of the ( $\nu$ )SMEFT up to dimension seven and assume the existence of  $n$  HNLs, one of which is in the mass range 10 – 100 GeV, within the kinematic reach of the EIC. In this context, HNLs can be produced at the EIC via mixing with light neutrinos (see Fig. 1) or via higher-dimensional operators. In this exploratory study, we focused on the mixing mechanism, assessed the sensitivity of the EIC, and compared it to other probes of HNLs.

In Section 3, we have presented a detailed study of the HNL-induced process  $e^-p \rightarrow \ell_\alpha^+ + k j + X$  and the corresponding Standard Model backgrounds (see Figs. 2, 3, and 4). The kinematic distributions presented in Fig. 2 for the electron flavor channel are somewhat different from the ones presented in Ref. [18]. This difference originates from our more stringent generator-level cuts on the jet  $p_T$  and our use of parton shower and detector response, which significantly extends the parton-level analysis of Ref. [18]. Based on the signal and background distributions, we have suggested a set of cuts for signal selection and background minimization (see Boxes I–IV), which provide the basis for a first sensitivity study.

Our analysis for the  $\mu$  and  $\tau$  channels  $e^-p \rightarrow \ell_\alpha^+ + k j + X$  ( $\alpha \in \{\mu, \tau\}$ ) assumes a muon detection efficiency comparable to the electron detection efficiencies. We emphasize here that the muon channel  $e^-p \rightarrow \mu^+ j j(j)$  benefits from a particularly clean experimental signature. This underscores the importance of muon identification capabilities at the EIC [42–44], to extend the reach of this machine to BSM physics. Our analysis of the  $\tau$  channel at the moment relies on reconstructing the  $\tau$  through its leptonic decay into a muon and neutrinos. The muon  $p_T$  distribution resulting from the  $e^-p \rightarrow \tau^+ j j(j)$  signal events is softer than the one from  $e^-p \rightarrow \mu^+ j j(j)$ , and thus the  $\tau$  channel suffers from intrinsic Standard Model backgrounds. Reconstruction of the  $\tau$  from hadronic decays can dramatically improve the sensitivity in the  $\tau$  channel, through background reduction and larger branching fractions.

In Section 4 we illustrated the reach of the EIC in probing HNL mixing angles in the mass range  $m_4 \in [10, 100]$  GeV. We first considered a scenario in which indirect constraints from low-energy probes can be canceled by  $(\nu)$ SMEFT operators (Figs. 5 - 7). Our results show that the EIC with muon detection capabilities and an integrated luminosity of  $100 \text{ fb}^{-1}$  can be competitive with the LHC <sup>7</sup>. We then considered a more restrictive  $3 + 1$  scenario with no  $(\nu)$ SMEFT contributions (Figs. 8 - 10). In this case constraints from other probes are stronger than the projected upper bound on the sensitivity from the EIC by an order of magnitude or more. On the other hand, the EIC processes have a comparable sensitivity to  $\mu \rightarrow e$  conversion in the range  $m_4 = (20 - 60)$  GeV and are more sensitive than  $\tau \rightarrow e\gamma$ .

Our exploratory study motivates further experimental assessment of both muon detection capabilities and  $\tau$  hadronic reconstruction, as well as further theoretical investigations. In particular, our findings motivate a more general theoretical analysis in which the  $(\nu)$ SMEFT operators that can interfere with resonant production at colliders (LHC, EIC) and with the strongest probes at lower energies are simultaneously turned on. In this more general  $(\nu)$ SMEFT framework, the EIC can play a central role. In fact, for resonant production at colliders, given the different energy scales involved, we expect that the relative importance of the mixing mechanism and dim-6 and dim-7  $(\nu)$ SMEFT operators will differ between the EIC and the LHC. Therefore, given that we find constraints from the EIC and the LHC to be within  $\mathcal{O}(1)$ , searches in all these channels will provide multiple paths to discovery and ways to disentangle the origin of a possible positive signal or fully constrain the parameter space in case of null results.

## Acknowledgments

We thank Zuhail Demiroglu, Abhay Deshpande, Ciprian Gal, Charlotte Van Hulse, Krishna Kumar, Ming Liu, Rafael Coelho Lopes de Sá, Frank Petriello, Richard Ruiz, and Zhoudunming Tu for valuable discussions and correspondence on various aspects of this work. V.C., W.D., and S.U.Q. gratefully acknowledge support from the U.S. DOE under Grant No. DE-FG02-00ER41132. E.M. gratefully acknowledges financial support by Los Alamos National Laboratory’s Laboratory Directed Research and Development program under project 20250164ER. Los Alamos National Laboratory is operated by Triad National Security, LLC, for the National Nuclear Security Administration of U.S. Department of Energy (Contract No. 89233218CNA000001). K. F. acknowledges the support by RIKEN iTHEMS SUURI-COOL (KEK) program.

---

<sup>7</sup>We base this conclusion on the existing analysis of Ref. [67] and projecting improvements that scale with the inverse square root of the integrated luminosity.

## A Constraints on HNLs from other processes

### A.1 LEP and LHC constraints

The decay of the  $Z$  boson to a HNL provides strong constraints on  $\sum_{i<4} \left| \sum_{\alpha} U_{\alpha i}^* U_{\alpha 4} \right|^2 \simeq \sum_{\alpha} |U_{\alpha 4}|^2$ , where  $\alpha = \{e, \mu, \tau\}$ . The non-observation of  $Z \rightarrow \nu_i N_4$  with  $i < 4$  at LEP [73] bounds this combination at the level of  $2 \times 10^{-5}$  for  $m_4 < 80$  GeV. In addition, CMS and ATLAS have performed searches for  $W$  production followed by  $W \rightarrow N_4 \ell$  [71, 72], which probe the combinations of couplings  $|U_{\alpha 4}|^4 / U_4^2$ . For  $\alpha = \mu$ , the results, combined with the LEP limits, provide a slightly more stringent bound on  $|U_{\mu 4}|$ .

### A.2 Weak charged-current decays

Weak decays of mesons and leptons with masses smaller than  $m_4$  constrain the absolute value of mixing angles  $|U_{\alpha 4}|$  independently of  $m_4$ . The effect of the mixing angles shows up both directly, by contributing to the relevant rates, and indirectly, by modifying the measured Fermi constant. In particular, the Fermi constant extracted from muon decay  $G_{\mu}$  is related to  $G_F$  appearing in semileptonic decays via [74, 75]

$$G_{\mu}^2 = G_F^2 (1 - |U_{e4}|^2)(1 - |U_{\mu 4}|^2). \quad (\text{A.1})$$

The combination of direct and indirect effects in the rate of semileptonic decays involving the underlying quarks  $d_j$   $u_i$  and leptons  $\ell_{\alpha}$ ,  $\bar{\nu}_{\alpha}$  then scales as

$$\Gamma_{u_i, d_j, \ell_{\alpha}, \nu_{\alpha}} \propto G_F^2 |V_{u_i d_j}|^2 (1 - |U_{\alpha 4}|^2) = G_{\mu}^2 |V_{u_i d_j}|^2 \frac{1 - |U_{\alpha 4}|^2}{(1 - |U_{e4}|^2)(1 - |U_{\mu 4}|^2)}, \quad (\text{A.2})$$

where  $V_{u_i d_j}$  denotes a generic element of the Cabibbo-Kobayashi-Maskawa (CKM) matrix.

The strongest constraints on the mixing angle come from tests of unitarity of the CKM matrix and from lepton universality tests. For CKM unitarity, the effective channel-dependent CKM elements extracted from the decay rate  $\Gamma_{u_i, d_j, \ell_{\alpha}, \nu_{\alpha}}$  read, for small mixing,

$$\bar{V}_{u_i d_j} = V_{u_i d_j} \times \left( 1 + \frac{1}{2} (|U_{e4}|^2 + |U_{\mu 4}|^2 - |U_{\alpha 4}|^2) \right). \quad (\text{A.3})$$

To set constraints, we use extraction of  $\bar{V}_{us}$  from  $K \rightarrow \pi \mu \nu$  and  $K \rightarrow \pi e \nu$  decays, which are given for electron and muon channels in Refs. [53, 76]. For the kaon form factor at zero momentum,  $f_+(0)$ , we use the average of  $N_f = 2 + 1 + 1$  lattice QCD calculations [77–79]. In addition, we use the ratio  $\Gamma(K \rightarrow \mu \nu) / \Gamma(\pi \rightarrow \mu \nu)$ , to obtain [77]

$$\frac{|\bar{V}_{us}|}{|\bar{V}_{ud}|} = 0.23126(51), \quad (\text{A.4})$$

using the lattice QCD determination of the ratio of  $f_K / f_{\pi}$  [77, 80–84]. Finally, we determine  $\bar{V}_{ud}$  from superallowed  $\beta$  decays [53, 85]

$$|\bar{V}_{ud}| = 0.97367(32). \quad (\text{A.5})$$

This determination only involves  $\alpha = e$ , and thus is sensitive to  $|U_{\mu 4}|^2$ .

Lepton flavor universality tests involve the ratios  $\mathcal{R}_{\alpha\beta} = \Gamma_{u_i, d_j, \ell_\alpha, \nu_\alpha} / \Gamma_{u_i, d_j, \ell_\beta, \nu_\beta}$ , which can be re-expressed as

$$\mathcal{R}_{\alpha\beta} = \mathcal{R}_{\alpha\beta} \Big|_{\text{SM}} (1 - |U_{\alpha 4}|^2 + |U_{\beta 4}|^2) . \quad (\text{A.6})$$

Similarly, for leptonic  $\tau$  decays, one finds [86]

$$R_{\mu/e}^\tau = \frac{\Gamma(\tau \rightarrow \mu \bar{\nu}_\mu \nu_\tau)}{\Gamma(\tau \rightarrow e \bar{\nu}_e \nu_\tau)} = R_{\mu/e}^\tau \Big|_{\text{SM}} \frac{1 - |U_{\mu 4}|^2}{1 - |U_{e 4}|^2}, \quad (\text{A.7})$$

$$R_{\tau/\mu}^\tau = \frac{\Gamma(\tau \rightarrow e \bar{\nu}_e \nu_\tau)}{\Gamma(\mu \rightarrow e \bar{\nu}_e \nu_\mu)} = R_{\tau/\mu}^\tau \Big|_{\text{SM}} \frac{1 - |U_{\tau 4}|^2}{1 - |U_{\mu 4}|^2}. \quad (\text{A.8})$$

In our analysis, we use ratios of  $\pi$  and  $K$  decays to muons and electrons,  $D_s$  meson decays to  $\tau$  and muons, and leptonic  $\tau$  decays. Theoretical input is taken from Refs. [86, 87].

We perform a fit to lepton universality and CKM unitarity observables, with four fit parameters:  $\lambda = V_{us}$  and the three mixing angles  $U_{\alpha 4}$ . We find that the  $\chi^2$  of the fit does not improve under the SM assumption, implying that adding HNLs to the theory does not resolve the Cabibbo anomaly. At the 95% confidence level, we obtain

$$|U_{e 4}|^2 < 3.7 \times 10^{-3} \quad (\text{A.9})$$

$$|U_{\mu 4}|^2 < 3.8 \times 10^{-4} \quad (\text{A.10})$$

$$|U_{\tau 4}|^2 < 4.1 \times 10^{-3}. \quad (\text{A.11})$$

### A.3 LFV and LNV decays

The rate for the decays (LFV or LNV) of mesons, leptons, or the  $Z$  boson, involving flavors  $\alpha$  and  $\beta$  takes the form

$$\Gamma_{\alpha\beta}^{(i)} = \gamma^{(i)} (|U_{\alpha 4}| |U_{\beta 4}|)^2 g^{(i)}(m_4) . \quad (\text{A.12})$$

The LNV decays are induced by dimension-9 operators that arise at tree level, leading to the scaling  $g^{(i)} = 1/m_4^2$ , while  $g^{(i)}$  is a function of  $(M_W/m_4)$  for LFV decays, which arise a loop-level. Below, we discuss the resulting constraints.

- **LFV  $\mu$  and  $\tau$  decays:** In the  $\mu - e$  sector, the strongest constraints arise from  $\mu \rightarrow e\gamma$  and  $\mu \rightarrow e$  conversion in nuclei. Using results from Ref. [88], where all the relevant decay rates have been computed, we update the limits. We find that, for the mass range of interest, the strongest constraints arise from  $\mu \rightarrow e$  conversion in gold [89] and titanium [90], followed by  $\mu \rightarrow e\gamma$  [91]. In the  $\tau - e$  sector, many LFV decay modes are available. We take as a representative the radiative mode  $\tau \rightarrow e\gamma$  for which a 90% CL upper limit of  $3.3 \times 10^{-8}$  has been set in Ref. [92].
- **$\mu^- \rightarrow e^+$  conversion:** Here the theoretical uncertainties are larger. Ref. [93] provided an estimate of the decay rate based on dimensional analysis, in terms of an undetermined scale  $Q \sim m_\mu$ . Using this approach, we obtain the weak bound

$$|U_{e 4} U_{\mu 4}| \leq 4.25 \left( \frac{m_\mu}{Q} \right)^3 \frac{m_4}{\text{GeV}} . \quad (\text{A.13})$$

On the other hand, Ref. [94] performed a calculation of the nuclear matrix elements induced by the exchange of Majorana neutrinos (light or heavy). Using their results, we obtain the even weaker limit

$$|U_{e4}U_{\mu4}| \leq 3 \times 10^4 \frac{m_4}{\text{GeV}} . \quad (\text{A.14})$$

- **LNV  $\tau$  decays:** Ref. [95] studied LNV  $\tau$  decays induced by dimension-7 in the SMEFT, which in turn generate dim-6 and dim-9 operators in the LEFT. Using the results of Ref. [95] for the hadronic matrix element, from the process  $\tau^\pm \rightarrow e^\mp \pi^\pm \pi^\pm$  we obtain the very loose bound

$$|U_{e4}U_{\tau4}| \leq 6.2 \times 10^3 \frac{m_4}{\text{GeV}} . \quad (\text{A.15})$$

#### A.4 Neutrino-less double beta decay

We compute the decay rate due to LNV from both light neutrinos and  $N_4$ , which induces a dimension-9 operator at low energy [96]. Treating the  $N_4$  and  $m_{\beta\beta}$  contributions as independent, and focusing on the  $^{136}\text{Xe}$  isotope for which the strongest half-life bound is currently available [97], we obtain [98]

$$\left[ T_{1/2}^{0\nu} (^{136}\text{Xe}) \right]^{-1} = \left[ a |\bar{m}_{\beta\beta}|^2 + b \frac{|m_{\beta\beta}| |U_{e4}|^2}{\bar{m}_4} \cos \eta + c \left( \frac{|U_{e4}|^2}{\bar{m}_4} \right)^2 \right] \text{yr}^{-1} , \quad (\text{A.16})$$

where  $\bar{m}_{\beta\beta} = m_{\beta\beta}/\text{eV}$ ,  $\bar{m}_4 = m_4/\text{GeV}$ , and  $\eta$  is the unconstrained relative phase between  $m_{\beta\beta}$  and  $U_{e4}^2$ . Using the nuclear matrix elements of Ref. [99] and the phase space factors extracted from Ref. [100] one obtains  $a = 2.4 \times 10^{-24}$ ,  $b = 1.5 \times 10^{-16}$ ,  $c = 2.3 \times 10^{-9}$ . The strongest constraint on the  $0\nu\beta\beta$  decay half-life comes from the 2024 KamLAND-Zen measurement [97], which implies the lower limit  $T_{1/2}^{0\nu} (^{136}\text{Xe}) > 4.4 \times 10^{26}$  yr at 95% C.L.

For  $\cos \eta > 0$ , marginalizing over  $m_{\beta\beta}$  we obtain  $|U_{e4}|^2 < 1.1 \times 10^{-9} m_4/\text{GeV}$ , where the upper limit is reached for  $m_{\beta\beta} \rightarrow 0$ . For  $\cos \eta < 0$  cancellations are possible. In particular, for  $\cos^2 \eta < \cos^2 \eta_0 = 4ac/b^2$  ( $= 0.98133$  with the matrix elements we use) a flat direction opens up, implying the contributions to  $0\nu\beta\beta$  are canceled when  $|U_{e4}|^2/\bar{m}_4 < b/(2c)(1 + \sqrt{1 - 4ca/b^2}) |\bar{m}_{\beta\beta}| \approx 3.8 \times 10^{-8} |\bar{m}_{\beta\beta}|$ . While this could in principle relax the bound on  $|U_{e4}|^2/m_4$ , in practice the effect is minimal, given the small coefficient  $\sim 10^{-8}$  and the fact that  $|m_{\beta\beta}|$  itself is indirectly bound by tritium beta decay and cosmology, through its correlation with  $m_\beta = \sqrt{\sum_{i=1}^3 |U_{ei}|^2 m_i^2}$  and  $\Sigma = \sum_{i=1}^3 m_i$ . The current bounds on  $m_\beta$  [101] and  $\Sigma$  [102] roughly translate into upper bounds  $|m_{\beta\beta}| < 0.5$  eV and  $|m_{\beta\beta}| < 0.061$  eV, respectively<sup>8</sup>. We show the allowed region in the parameter space of  $|U_{e4}|^2$  vs  $m_4$  in Fig. 11. Here, the blue (red) shaded region denotes the combination of  $0\nu\beta\beta$  and the KATRIN measurement (cosmological constraints). The bound on the HNL coupling and mass relaxes by at most one order of magnitude compared to the  $|m_{\beta\beta}| = 0$  case. Using only the KATRIN constraint

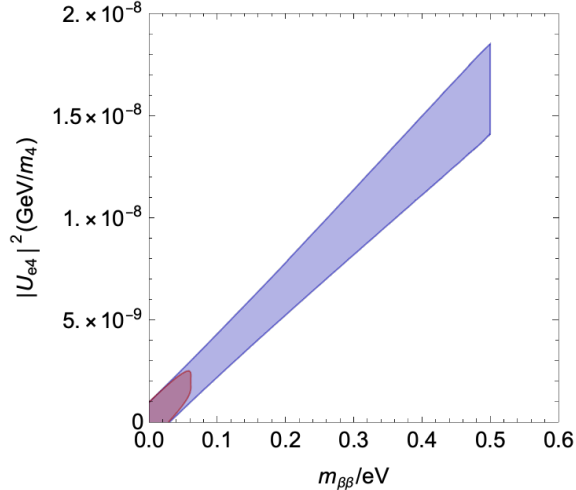


**Figure 11.** Allowed region obtained from the combination of  $0\nu\beta\beta$  constraints with the KATRIN (cosmological) bound in blue (red). After marginalizing over the phases, the limits from KATRIN and cosmology provide an upper limit on  $m_{\beta\beta}$ . The contours are obtained from  $\chi^2 = \left(T_{1/2}^{0\nu}/T_{1/2}^{0\nu(\text{expt})}\right)^2 + \left(m_{\beta\beta}/m_{\beta\beta}^{(\text{expt})}\right)^2$ , where  $m_{\beta\beta}^{(\text{expt})}$  refers to the upper limits from either the KATRIN experiment or cosmology.

on  $|m_{\beta\beta}|$  leads to  $|U_{e4}|^2 < 1.5 \times 10^{-8} m_4/\text{GeV}$ . We used the combination of  $0\nu\beta\beta$  and the constraints from KATRIN to obtain the sensitivity plots in the main text.

## References

- [1] S. Weinberg, *Baryon and Lepton Nonconserving Processes*, *Phys. Rev. Lett.* **43** (1979) 1566–1570.
- [2] P. Fileviez Perez et al., *On Baryon and Lepton Number Violation*, [2208.00010](#).
- [3] M. Agostini, G. Benato, J. A. Detwiler, J. Menéndez and F. Vissani, *Toward the discovery of matter creation with neutrinoless  $\beta\beta$  decay*, *Rev. Mod. Phys.* **95** (2023) 025002, [[2202.01787](#)].
- [4] P. Minkowski,  *$\mu \rightarrow e\gamma$  at a Rate of One Out of  $10^9$  Muon Decays?*, *Phys. Lett. B* **67** (1977) 421–428.
- [5] M. Gell-Mann, P. Ramond and R. Slansky, *Complex Spinors and Unified Theories*, *Conf. Proc. C* **790927** (1979) 315–321, [[1306.4669](#)].
- [6] T. Yanagida, *Horizontal gauge symmetry and masses of neutrinos*, *Conf. Proc. C* **7902131** (1979) 95–99.
- [7] S. L. Glashow, *The Future of Elementary Particle Physics*, *NATO Sci. Ser. B* **61** (1980) 687.

---

<sup>8</sup>For  $m_4$  in the 10-100 GeV region, as considered here, the contribution of the Heavy Neutral Lepton does not impact the analysis of tritium decay and the cosmological signatures of light neutrino mass.

- [8] R. N. Mohapatra and G. Senjanovic, *Neutrino Mass and Spontaneous Parity Violation*, *Phys. Rev. Lett.* **44** (1980) 912.
- [9] A. M. Abdullahi et al., *The present and future status of heavy neutral leptons*, *J. Phys. G* **50** (2023) 020501, [2203.08039].
- [10] R. Abdul Khalek et al., *Science Requirements and Detector Concepts for the Electron-Ion Collider: EIC Yellow Report*, *Nucl. Phys. A* **1026** (2022) 122447, [2103.05419].
- [11] W. Buchmuller and C. Greub, *Heavy Majorana neutrinos in electron - positron and electron - proton collisions*, *Nucl. Phys. B* **363** (1991) 345–368.
- [12] W. Buchmuller and C. Greub, *Right-handed currents and heavy neutrinos in high-energy ep and  $e^+e^-$  scattering*, *Nucl. Phys. B* **381** (1992) 109–128.
- [13] G. Ingelman and J. Rathsmann, *Heavy Majorana neutrinos at e p colliders*, *Z. Phys. C* **60** (1993) 243–254.
- [14] C. Blaksley, M. Blennow, F. Bonnet, P. Coloma and E. Fernandez-Martinez, *Heavy Neutrinos and Lepton Number Violation in lp Colliders*, *Nucl. Phys. B* **852** (2011) 353–365, [1105.0308].
- [15] L. Duarte, G. A. González-Sprinberg and O. A. Sampayo, *Majorana neutrinos production at LHeC in an effective approach*, *Phys. Rev. D* **91** (2015) 053007, [1412.1433].
- [16] S. Mondal and S. K. Rai, *Polarized window for left-right symmetry and a right-handed neutrino at the Large Hadron-Electron Collider*, *Phys. Rev. D* **93** (2016) 011702, [1510.08632].
- [17] M. Lindner, F. S. Queiroz, W. Rodejohann and C. E. Yaguna, *Left-Right Symmetry and Lepton Number Violation at the Large Hadron Electron Collider*, *JHEP* **06** (2016) 140, [1604.08596].
- [18] B. Batell, T. Ghosh, T. Han and K. Xie, *Heavy neutral leptons at the Electron-Ion Collider*, *JHEP* **03** (2023) 020, [2210.09287].
- [19] F. del Aguila, S. Bar-Shalom, A. Soni and J. Wudka, *Heavy Majorana Neutrinos in the Effective Lagrangian Description: Application to Hadron Colliders*, *Phys. Lett. B* **670** (2009) 399–402, [0806.0876].
- [20] Y. Liao and X.-D. Ma, *Operators up to Dimension Seven in Standard Model Effective Field Theory Extended with Sterile Neutrinos*, *Phys. Rev. D* **96** (2017) 015012, [1612.04527].
- [21] A. Aparici, K. Kim, A. Santamaria and J. Wudka, *Right-handed neutrino magnetic moments*, *Phys. Rev. D* **80** (2009) 013010, [0904.3244].
- [22] B. Grzadkowski, M. Iskrzynski, M. Misiak and J. Rosiek, *Dimension-Six Terms in the Standard Model Lagrangian*, *JHEP* **1010** (2010) 085, [1008.4884].
- [23] L. Lehman, *Extending the Standard Model Effective Field Theory with the Complete Set of Dimension-7 Operators*, *Phys. Rev. D* **90** (2014) 125023, [1410.4193].
- [24] KATRIN collaboration, M. Aker et al., *Improved Upper Limit on the Neutrino Mass from a Direct Kinematic Method by KATRIN*, *Phys. Rev. Lett.* **123** (2019) 221802, [1909.06048].
- [25] A. Atre, T. Han, S. Pascoli and B. Zhang, *The Search for Heavy Majorana Neutrinos*, *JHEP* **05** (2009) 030, [0901.3589].

- [26] M. Drewes and B. Garbrecht, *Combining experimental and cosmological constraints on heavy neutrinos*, *Nucl. Phys. B* **921** (2017) 250–315, [[1502.00477](#)].
- [27] A. Abada, V. De Romeri, M. Lucente, A. M. Teixeira and T. Toma, *Effective Majorana mass matrix from tau and pseudoscalar meson lepton number violating decays*, *JHEP* **02** (2018) 169, [[1712.03984](#)].
- [28] P. D. Bolton, F. F. Deppisch and P. S. Bhupal Dev, *Neutrinoless double beta decay versus other probes of heavy sterile neutrinos*, *JHEP* **03** (2020) 170, [[1912.03058](#)].
- [29] F. M. L. Almeida, J. A. Martins Simoes and A. J. Ramalho, *Heavy lepton production in E P collisions*, *Nucl. Phys. B* **347** (1990) 537–549.
- [30] H1 collaboration, F. D. Aaron et al., *A Search for Excited Neutrinos in e- p Collisions at HERA*, *Phys. Lett. B* **663** (2008) 382–389, [[0802.1858](#)].
- [31] O. Mattelaer, M. Mitra and R. Ruiz, *Automated Neutrino Jet and Top Jet Predictions at Next-to-Leading-Order with Parton Shower Matching in Effective Left-Right Symmetric Models*, [1610.08985](#).
- [32] S. Antusch, E. Cazzato and O. Fischer, *Sterile neutrino searches at future e<sup>-</sup>e<sup>+</sup>, pp, and e<sup>-</sup>p colliders*, *Int. J. Mod. Phys. A* **32** (2017) 1750078, [[1612.02728](#)].
- [33] J. Alwall, R. Frederix, S. Frixione, V. Hirschi, F. Maltoni, O. Mattelaer et al., *The automated computation of tree-level and next-to-leading order differential cross sections, and their matching to parton shower simulations*, *JHEP* **07** (2014) 079, [[1405.0301](#)].
- [34] C. Bierlich et al., *A comprehensive guide to the physics and usage of PYTHIA 8.3*, *SciPost Phys. Codeb.* **2022** (2022) 8, [[2203.11601](#)].
- [35] A. Alloul, N. D. Christensen, C. Degrande, C. Duhr and B. Fuks, *FeynRules 2.0 - A complete toolbox for tree-level phenomenology*, *Comput. Phys. Commun.* **185** (2014) 2250–2300, [[1310.1921](#)].
- [36] D. Alva, T. Han and R. Ruiz, *Heavy Majorana neutrinos from Wγ fusion at hadron colliders*, *JHEP* **02** (2015) 072, [[1411.7305](#)].
- [37] C. Degrande, O. Mattelaer, R. Ruiz and J. Turner, *Fully-Automated Precision Predictions for Heavy Neutrino Production Mechanisms at Hadron Colliders*, *Phys. Rev. D* **94** (2016) 053002, [[1602.06957](#)].
- [38] R. Abdul Khalek et al., *Science Requirements and Detector Concepts for the Electron-Ion Collider: EIC Yellow Report*, *Nucl. Phys. A* **1026** (2022) 122447, [[2103.05419](#)].
- [39] DELPHES 3 collaboration, J. de Favereau, C. Delaere, P. Demin, A. Giammanco, V. Lemaître, A. Mertens et al., *DELPHES 3, A modular framework for fast simulation of a generic collider experiment*, *JHEP* **02** (2014) 057, [[1307.6346](#)].
- [40] M. Arratia, Y. Furetova, T. J. Hobbs, F. Olness and S. J. Sekula, *Charm jets as a probe for strangeness at the future Electron-Ion Collider*, *Phys. Rev. D* **103** (2021) 074023, [[2006.12520](#)].
- [41] M. Arratia and S. Sekula, *A Delphes card for the EIC yellow-report detector*, [2103.06886](#).
- [42] P. D. Grannis and H. E. Montgomery, *Motivation for Two Detectors at a Particle Physics Collider*, [2303.08228](#).

- [43] P. Nadel-Turonski, *A Second Detector for the Electron-Ion Collider*, *PoS DIS2024* (2025) 283.
- [44] J. Kim, *Overview on Efforts for a Second Detector at the Electron-Ion Collider (EIC)*, vol. DIS2025, p. 133, 2025. [2509.24983](#). DOI.
- [45] D0 collaboration, B. Abbott et al., *Differential Cross Section for W Boson Production as a Function of Transverse Momentum in  $p\bar{p}$  Collisions at  $\sqrt{s} = 1.8$  TeV*, *Phys. Lett. B* **513** (2001) 292–300, [[hep-ex/0010026](#)].
- [46] S. Pascoli, R. Ruiz and C. Weiland, *Heavy neutrinos with dynamic jet vetoes: multilepton searches at  $\sqrt{s} = 14$ , 27, and 100 TeV*, *JHEP* **06** (2019) 049, [[1812.08750](#)].
- [47] D. Gorbunov and M. Shaposhnikov, *How to find neutral leptons of the  $\nu$ MSM?*, *JHEP* **10** (2007) 015, [[0705.1729](#)].
- [48] J. C. Helo, S. Kovalenko and I. Schmidt, *Sterile neutrinos in lepton number and lepton flavor violating decays*, *Nucl. Phys. B* **853** (2011) 80–104, [[1005.1607](#)].
- [49] B. Shuve and M. E. Peskin, *Revision of the LHCb Limit on Majorana Neutrinos*, *Phys. Rev. D* **94** (2016) 113007, [[1607.04258](#)].
- [50] K. Bondarenko, A. Boyarsky, D. Gorbunov and O. Ruchayskiy, *Phenomenology of GeV-scale Heavy Neutral Leptons*, *JHEP* **11** (2018) 032, [[1805.08567](#)].
- [51] Y.-F. Shen and A. Gurrola, *Large-Width New Physics at Colliders: A Gauge-Invariant Resummation Approach*, [2511.15114](#).
- [52] A. Abada, P. Escribano, X. Marcano and G. Piazza, *Collider searches for heavy neutral leptons: beyond simplified scenarios*, *Eur. Phys. J. C* **82** (2022) 1030, [[2208.13882](#)].
- [53] PARTICLE DATA GROUP collaboration, S. Navas et al., *Review of particle physics*, *Phys. Rev. D* **110** (2024) 030001.
- [54] V. Cirigliano, K. Fuyuto, C. Lee, E. Mereghetti and B. Yan, *Charged Lepton Flavor Violation at the EIC*, *JHEP* **03** (2021) 256, [[2102.06176](#)].
- [55] ATLAS collaboration, M. Aaboud et al., *Search for doubly charged Higgs boson production in multi-lepton final states with the ATLAS detector using proton–proton collisions at  $\sqrt{s} = 13$  TeV*, *Eur. Phys. J. C* **78** (2018) 199, [[1710.09748](#)].
- [56] M. Muskinja, *Search for new physics processes with same charge leptons in the final state with the ATLAS detector using proton–proton collisions at  $\sqrt{s} = 13$  TeV*, Aug, 2018.
- [57] ATLAS collaboration, G. Aad et al., *Electron and photon performance measurements with the ATLAS detector using the 2015–2017 LHC proton–proton collision data*, *JINST* **14** (2019) P12006, [[1908.00005](#)].
- [58] J. D. Jackson, *Classical Electrodynamics*. Wiley, 1998.
- [59] J. Harz, M. J. Ramsey-Musolf, T. Shen and S. U. Quiroga, *TeV-scale lepton number violation: Connecting leptogenesis, neutrinoless double beta decay, and colliders*, *Phys. Rev. D* **110** (2024) 035024, [[2106.10838](#)].
- [60] X. Li, *Recent open heavy flavor studies for the Electron-Ion Collider*, *PoS QNP2024* (2025) 113, [[2501.18044](#)].

- [61] S. Frixione, M. L. Mangano, P. Nason and G. Ridolfi, *Improving the Weizsacker-Williams approximation in electron - proton collisions*, *Phys. Lett. B* **319** (1993) 339–345, [[hep-ph/9310350](#)].
- [62] M. Blennow, E. Fernández-Martínez, J. Hernández-García, J. López-Pavón, X. Marcano and D. Naredo-Tuero, *Bounds on lepton non-unitarity and heavy neutrino mixing*, *JHEP* **08** (2023) 030, [[2306.01040](#)].
- [63] E. Fernández-Martínez, M. González-López, J. Hernández-García, M. Hostert and J. López-Pavón, *Effective portals to heavy neutral leptons*, *JHEP* **09** (2023) 001, [[2304.06772](#)].
- [64] V. Cirigliano, J. Jenkins and M. González-Alonso, *Semileptonic decays of light quarks beyond the Standard Model*, *Nucl. Phys.* **B830** (2010) 95–115, [[0908.1754](#)].
- [65] M. González-Alonso, J. Martin Camalich and K. Mimouni, *Renormalization-group evolution of new physics contributions to (semi)leptonic meson decays*, *Phys. Lett. B* **772** (2017) 777–785, [[1706.00410](#)].
- [66] V. Cirigliano, W. Dekens, J. de Vries, M. L. Graesser and E. Mereghetti, *Neutrinoless double beta decay in chiral effective field theory: lepton number violation at dimension seven*, *JHEP* **12** (2017) 082, [[1708.09390](#)].
- [67] CMS collaboration, A. M. Sirunyan et al., *Search for heavy Majorana neutrinos in same-sign dilepton channels in proton-proton collisions at  $\sqrt{s} = 13$  TeV*, *JHEP* **01** (2019) 122, [[1806.10905](#)].
- [68] PARTICLE DATA GROUP collaboration, P. A. Zyla et al., *Review of Particle Physics*, *PTEP* **2020** (2020) 083C01.
- [69] ATLAS collaboration, G. Aad et al., *Search for heavy Majorana neutrinos with the ATLAS detector in pp collisions at  $\sqrt{s} = 8$  TeV*, *JHEP* **07** (2015) 162, [[1506.06020](#)].
- [70] ATLAS collaboration, G. Aad et al., *Search for heavy neutral leptons in decays of W bosons produced in 13 TeV pp collisions using prompt and displaced signatures with the ATLAS detector*, *JHEP* **10** (2019) 265, [[1905.09787](#)].
- [71] CMS collaboration, A. Hayrapetyan et al., *Search for heavy neutral leptons in final states with electrons, muons, and hadronically decaying tau leptons in proton-proton collisions at  $\sqrt{s} = 13$  TeV*, *JHEP* **06** (2024) 123, [[2403.00100](#)].
- [72] ATLAS collaboration, G. Aad et al., *Search for heavy neutral leptons in decays of W bosons produced in 13 TeV pp collisions using prompt signatures in the ATLAS detector*, *Eur. Phys. J. C* **86** (2026) 153, [[2508.20929](#)].
- [73] DELPHI collaboration, P. Abreu et al., *Search for neutral heavy leptons produced in Z decays*, *Z. Phys. C* **74** (1997) 57–71.
- [74] E. Fernandez-Martinez, J. Hernandez-Garcia and J. Lopez-Pavon, *Global constraints on heavy neutrino mixing*, *JHEP* **08** (2016) 033, [[1605.08774](#)].
- [75] M. Blennow, P. Coloma, E. Fernandez-Martinez, J. Hernandez-Garcia and J. Lopez-Pavon, *Non-Unitarity, sterile neutrinos, and Non-Standard neutrino Interactions*, *JHEP* **04** (2017) 153, [[1609.08637](#)].

- [76] M. Moulson, “Kaon decays and the cabibbo angle anomaly.” <https://indico.cern.ch/event/1184945/contributions/5540813/attachments/2717802/4721036/CKM%202023.pdf>.
- [77] FLAVOUR LATTICE AVERAGING GROUP (FLAG) collaboration, Y. Aoki et al., *FLAG review 2024*, *Phys. Rev. D* **113** (2026) 014508, [2411.04268].
- [78] N. Carrasco, P. Lami, V. Lubicz, L. Riggio, S. Simula and C. Tarantino, *K* →  $\pi$  semileptonic form factors with  $N_f = 2 + 1 + 1$  twisted mass fermions, *Phys. Rev. D* **93** (2016) 114512, [1602.04113].
- [79] FERMILAB LATTICE, MILC collaboration, A. Bazavov et al.,  $|V_{us}|$  from  $K_{\ell 3}$  decay and four-flavor lattice QCD, *Phys. Rev. D* **99** (2019) 114509, [1809.02827].
- [80] R. J. Dowdall, C. T. H. Davies, G. P. Lepage and C. McNeile,  $V_{us}$  from  $\pi$  and  $K$  decay constants in full lattice QCD with physical  $u$ ,  $d$ ,  $s$  and  $c$  quarks, *Phys. Rev. D* **88** (2013) 074504, [1303.1670].
- [81] N. Carrasco et al., *Leptonic decay constants  $f_K$ ,  $f_D$ , and  $f_{D_s}$  with  $N_f = 2 + 1 + 1$  twisted-mass lattice QCD*, *Phys. Rev. D* **91** (2015) 054507, [1411.7908].
- [82] A. Bazavov et al., *B- and D-meson leptonic decay constants from four-flavor lattice QCD*, *Phys. Rev. D* **98** (2018) 074512, [1712.09262].
- [83] N. Miller et al.,  *$F_K/F_\pi$  from Möbius Domain-Wall fermions solved on gradient-flowed HISQ ensembles*, *Phys. Rev. D* **102** (2020) 034507, [2005.04795].
- [84] EXTENDED TWISTED MASS collaboration, C. Alexandrou et al., *Ratio of kaon and pion leptonic decay constants with  $N_f=2+1+1$  Wilson-clover twisted-mass fermions*, *Phys. Rev. D* **104** (2021) 074520, [2104.06747].
- [85] J. C. Hardy and I. S. Towner, *Superallowed  $0^+ \rightarrow 0^+$  nuclear  $\beta$  decays: 2020 critical survey, with implications for  $V_{ud}$  and CKM unitarity*, *Phys. Rev. C* **102** (2020) 045501.
- [86] D. Bryman, V. Cirigliano, A. Crivellin and G. Inguglia, *Testing Lepton Flavor Universality with Pion, Kaon, Tau, and Beta Decays*, *Ann. Rev. Nucl. Part. Sci.* **72** (2022) 69–91, [2111.05338].
- [87] A. Pich, *Precision Tau Physics*, *Prog. Part. Nucl. Phys.* **75** (2014) 41–85, [1310.7922].
- [88] R. Alonso, M. Dhen, M. B. Gavela and T. Hambye, *Muon conversion to electron in nuclei in type-I seesaw models*, *JHEP* **01** (2013) 118, [1209.2679].
- [89] SINDRUM II collaboration, W. H. Bertl et al., *A Search for muon to electron conversion in muonic gold*, *Eur. Phys. J. C* **47** (2006) 337–346.
- [90] SINDRUM II collaboration, C. Dohmen et al., *Test of lepton flavor conservation in  $\mu \rightarrow e$  conversion on titanium*, *Phys. Lett. B* **317** (1993) 631–636.
- [91] MEG II collaboration, K. Afanaciev et al., *A search for  $\mu^+ \rightarrow e^+\gamma$  with the first dataset of the MEG II experiment*, *Eur. Phys. J. C* **84** (2024) 216, [2310.12614].
- [92] BABAR collaboration, B. Aubert et al., *Searches for Lepton Flavor Violation in the Decays  $\tau^\pm \rightarrow e^\pm\gamma$  and  $\tau^\pm \rightarrow \mu^\pm\gamma$* , *Phys. Rev. Lett.* **104** (2010) 021802, [0908.2381].
- [93] J. M. Berryman, A. de Gouvêa, K. J. Kelly and A. Kobach, *Lepton-number-violating searches for muon to positron conversion*, *Phys. Rev. D* **95** (2017) 115010, [1611.00032].

- [94] P. Domin, S. Kovalenko, A. Faessler and F. Simkovic, *Nuclear ( $\mu^-$ ,  $e^+$ ) conversion mediated by Majorana neutrinos*, *Phys. Rev. C* **70** (2004) 065501, [[nucl-th/0409033](#)].
- [95] Y. Liao, X.-D. Ma and H.-L. Wang, *Effective field theory approach to lepton number violating  $\tau$  decays*, *Chin. Phys. C* **45** (2021) 073102, [[2102.03491](#)].
- [96] V. Cirigliano, W. Dekens, J. de Vries, M. L. Graesser and E. Mereghetti, *A neutrinoless double beta decay master formula from effective field theory*, *JHEP* **12** (2018) 097, [[1806.02780](#)].
- [97] KAMLAND-ZEN collaboration, S. Abe et al., *Search for Majorana Neutrinos with the Complete KamLAND-Zen Dataset*, *Phys. Rev. Lett.* **135** (2025) 262501, [[2406.11438](#)].
- [98] V. Cirigliano, W. Dekens, J. de Vries, K. Fuyuto, E. Mereghetti and R. Ruiz, *Leptonic anomalous magnetic moments in  $\nu$  SMEFT*, *JHEP* **08** (2021) 103, [[2105.11462](#)].
- [99] J. Hyvärinen and J. Suhonen, *Nuclear matrix elements for  $0\nu\beta\beta$  decays with light or heavy Majorana-neutrino exchange*, *Phys. Rev.* **C91** (2015) 024613.
- [100] M. Horoi and A. Neacsu, *Towards an effective field theory approach to the neutrinoless double-beta decay*, [[1706.05391](#)].
- [101] KATRIN collaboration, M. Aker et al., *Direct neutrino-mass measurement based on 259 days of KATRIN data*, *Science* **388** (2025) adq9592, [[2406.13516](#)].
- [102] DESI collaboration, A. G. Adame et al., *DESI 2024 VI: cosmological constraints from the measurements of baryon acoustic oscillations*, *JCAP* **02** (2025) 021, [[2404.03002](#)].